

POLITECNICO DI MILANO

Scuola di Ingegneria Industriale e dell'Informazione

Corso di Laurea Magistrale in
Physics Engineering



Simulation of Montel system

Relatore: Prof. Giacomo GHIRINGHELLI

Dott. Manuel SANCHEZ DEL RIO

Tesi di Laurea di:

Yiones AOUADI Matr. 872727

Anno Accademico 2017 - 2018

Yiones Aouadi: *Modello di Tesi di Laurea in L^AT_EX* | Tesi di Laurea Magistrale in
Engineering physics, Politecnico di Milano.
© Copyright Dicembre 2018.

Politecnico di Milano:
www.polimi.it

Scuola di Ingegneria Industriale e dell'Informazione:
www.ingindinf.polimi.it

Ringraziamenti

 Lorem ipsum dolor sit amet, consectetuer adipiscing elit. Ut purus elit, vestibulum ut, placerat ac, adipiscing vitae, felis. Curabitur dictum gravida mauris. Nam arcu libero, nonummy eget, consectetuer id, vulputate a, magna. Donec vehicula augue eu neque. Pellentesque habitant morbi tristique senectus et netus et malesuada fames ac turpis egestas. Mauris ut leo. Cras viverra metus rhoncus sem. Nulla et lectus vestibulum urna fringilla ultrices. Phasellus eu tellus sit amet tortor gravida placerat. Integer sapien est, iaculis in, pretium quis, viverra ac, nunc. Praesent eget sem vel leo ultrices bibendum. Aenean faucibus. Morbi dolor nulla, malesuada eu, pulvinar at, mollis ac, nulla. Curabitur auctor semper nulla. Donec varius orci eget risus. Duis nibh mi, congue eu, accumsan eleifend, sagittis quis, diam. Duis eget orci sit amet orci dignissim rutrum.

 Desidero inoltre ringraziare esplicitamente:

Esplicito1 per vari motivi;

Esplicito2 per altri motivi;

Esplicito3 per puro piacere, senza particolari motivi.

Milano, Dicembre 2018

L. M.

*a te,
ovunque tu sia,
e qualunque percorso di vita tu abbia intrapreso.*

Indice

Introduzione	1
1 Focusing for X-rays	3
1.1 Interaction with Matter	5
1.2 Total External Reflection	9
2 Mirrors for X-rays	17
2.1 Spherical surface	17
2.1.1 Astigmatism	17
2.1.2 Spherical Aberration	19
2.1.3 Reducing aberration	20
2.2 Conic Surfaces	20
2.3 Compound Optical system	22
2.3.1 Wolter System	22
2.3.2 Kirkpatrick-Baez System	23
2.4 Montel	24
2.4.1 Diffraction limit of Montel compared to sequential K:	24
2.4.2 Flux limit	28
2.4.3 Optical Design	28
3 MONWES	31
3.1 Beam	31
3.2 Optical Elements	35
3.2.1 Mirrors and lens	35
3.2.2 Compound Optical Element (KB and Montel system)	39
3.3 Tracing System	41
3.3.1 Tracing for simple Optical element	42
3.3.2 Tracing for KB	43
3.3.3 Tracing for Montel	43
4 Results	47
4.1 Testing	47
4.1.1 Testing with OASYS	47
4.1.2 Testing with the paper	50
4.2 Analysis of Montel system	50
4.2.1 Alignment	54
4.2.2 Alignment: Orthogonality	54

4.2.3	Alignment: Incidence angle	54
4.2.4	Alignment: point of incidence	54
A	Table for absorption coefficents	61
B	How to calculated the ellipse's and hyperbola's coefficients	65

Elenco delle figure

1.1 Attenuation coefficient for X-ray radiation of carbon 1.1a , and gold 1.1b	4
1.2 X-ray ionizing process	6
1.3 Interface of two medium	9
1.4 R_p 's values for grazing incidence with two values of δ , and some values of β	13
1.5 Ratio of $\frac{R_s}{R_p}$ for two values of δ , and some values of β	14
1.6 Reflectivity over the whole values of incidence angles	15
1.7 Slopes of reflectivity which show that, to have an inflection point, $\beta < 0.69\delta$	15
2.1 Formation image of a circular mirror	18
2.2 Image formation of a 3D spherical mirror	19
2.3 Different kind of surface conic, with the same c base curvature value, and different constant k	21
2.4 Example of spherical aberration correction	21
2.5 Sine Abbe condition for a lens	22
2.6 Kirkpatrick-Baez system	24
2.7 Montel system	24
2.8 Standard parameters that define an elliptical mirror	25
2.9 New parameter that define an elliptical mirror, useful for calculation	25
2.10 Plots	26
2.11 Plots	27
2.12 Example in how to build a Montel system starting from two cylindrical mirror cutting the edge with ad angle of 45°	29
3.1 Example of Beam definition	32
3.2 Example 1	32
3.3 Example 2	33
3.4 Example 3	33
3.5 Resume of the Beam object parameter	34
3.6 Parabola	36
3.7 System	37
3.8 Ellipse System	38
3.9 Hyperbola System	38
3.10 System	39
3.11 System	40

3.12 Example 5	40
3.13 System	41
3.14 Example 6	41
3.15 System	42
3.16 Example 7	42
3.17 Example 1	43
3.18 Example 8	43
3.19 Example 8	45
4.1 Optical system	48
4.2 Parameter of the source used for the comparison with OASYS	48
4.3 Parameter of the source used for the comparison with OASYS	49
4.4 Parameter of the source used for the comparison with OASYS	49
4.5 Parameter of the source used for the comparison with OASYS	49
4.6 Illustration of the Montel system used as a collimator in the paper [RKM15]	50
4.7 Results of the Montel simulations with a source beam with a FWHM spot of $2.5\mu\text{m}$ and a Gaussian divergence of 5mrad	51
4.8 Ideal system	52
4.9 Footprint, on the xy-mirror (4.13a) and on zy-mirror (4.13b). The red dots are those rays that hit before xy-mirror and after zy-mirror, the blue ones hit first xy-mirror and after zy-mirror.	53
4.10 Illumination at the image plane of the different Beam (red dots correspond to np-reflected rays, blue dot to one-reflected rays, green dots to two-reflected rays).	53
4.11 Histogram of x' after Montel	55
4.12 FWHM of x' after the Montel changing the orthogonality	56
4.13 Incidence angle	56
4.14 Different path for simulate the non-centred beam	57
4.15 Results of the Montel system of a source beam with a FWHM spot of $2.5\mu\text{m}$ and a Gaussian divergence of 5mrad	58
4.16 Results of the Montel system of a source beam with a FWHM spot of $2.5\mu\text{m}$ and a Gaussian divergence of 5mrad	59
B.1 Hyperbola's system	66
B.2 Hyperbola's system	67

Elenco delle tabelle

2.1 Parameter of different conic surfaces	20
---	----

Elenco dei codici

Sommario

Lorem ipsum dolor sit amet, consectetuer adipiscing elit. Ut purus elit, vestibulum ut, placerat ac, adipiscing vitae, felis. Curabitur dictum gravida mauris. Nam arcu libero, nonummy eget, consectetuer id, vulputate a, magna. Donec vehicula augue eu neque. Pellentesque habitant morbi tristique senectus et netus et malesuada fames ac turpis egestas. Mauris ut leo. Cras viverra metus rhoncus sem. Nulla et lectus vestibulum urna fringilla ultrices. Phasellus eu tellus sit amet tortor gravida placerat. Integer sapien est, iaculis in, pretium quis, viverra ac, nunc. Praesent eget sem vel leo ultrices bibendum. Aenean faucibus. Morbi dolor nulla, malesuada eu, pulvinar at, mollis ac, nulla. Curabitur auctor semper nulla. Donec varius orci eget risus. Duis nibh mi, congue eu, accumsan eleifend, sagittis quis, diam. Duis eget orci sit amet orci dignissim rutrum.

Nam dui ligula, fringilla a, euismod sodales, sollicitudin vel, wisi. Morbi auctor lorem non justo. Nam lacus libero, pretium at, lobortis vitae, ultricies et, tellus. Donec aliquet, tortor sed accumsan bibendum, erat ligula aliquet magna, vitae ornare odio metus a mi. Morbi ac orci et nisl hendrerit mollis. Suspendisse ut massa. Cras nec ante. Pellentesque a nulla. Cum sociis natoque penatibus et magnis dis parturient montes, nascetur ridiculus mus. Aliquam tincidunt urna. Nulla ullamcorper vestibulum turpis. Pellentesque cursus luctus mauris.

Parole chiave: PoliMi, Tesi, LaTeX, Scribd

Abstract

Text of the abstract in english...

Lorem ipsum dolor sit amet, consectetur adipiscing elit. Ut purus elit, vestibulum ut, placerat ac, adipiscing vitae, felis. Curabitur dictum gravida mauris. Nam arcu libero, nonummy eget, consectetur id, vulputate a, magna. Donec vehicula augue eu neque. Pellentesque habitant morbi tristique senectus et netus et malesuada fames ac turpis egestas. Mauris ut leo. Cras viverra metus rhoncus sem. Nulla et lectus vestibulum urna fringilla ultrices. Phasellus eu tellus sit amet tortor gravida placerat. Integer sapien est, iaculis in, pretium quis, viverra ac, nunc. Praesent eget sem vel leo ultrices bibendum. Aenean faucibus. Morbi dolor nulla, malesuada eu, pulvinar at, mollis ac, nulla. Curabitur auctor semper nulla. Donec varius orci eget risus. Duis nibh mi, congue eu, accumsan eleifend, sagittis quis, diam. Duis eget orci sit amet orci dignissim rutrum.

Nam dui ligula, fringilla a, euismod sodales, sollicitudin vel, wisi. Morbi auctor lorem non justo. Nam lacus libero, pretium at, lobortis vitae, ultricies et, tellus. Donec aliquet, tortor sed accumsan bibendum, erat ligula aliquet magna, vitae ornare odio metus a mi. Morbi ac orci et nisl hendrerit mollis. Suspendisse ut massa. Cras nec ante. Pellentesque a nulla. Cum sociis natoque penatibus et magnis dis parturient montes, nascetur ridiculus mus. Aliquam tincidunt urna. Nulla ullamcorper vestibulum turpis. Pellentesque cursus luctus mauris.

Keywords: PoliMi, Master Thesis, LaTeX, Scribd

Introduzione

The simulation of x-ray beam properties during the transport along a beamline is important for the design, the optimization and the operation of the beamline. The main optical element used for X-ray are curved mirrors, used in a grazing configuration, in order to focalize or collimate a beam. In a beam line are used simple mirrors or some particular kind of mirror combination that increase the performance of the optical system. An typical example is the Kirkpatrick-Baez (KB) system, very popular at the ESRF because of its many good properties and so well studied. However, the extreme quality of the synchrotron beams that will be available with the ESRF upgraded storage ring pushes the requirement in optics to consider more and more perfect elements. There is also another configuration of mirror, named "Montel" system, that should do the same work of the Kirkpatrick-Baez (KB) system.

During my traineeships at the ESRF I developed a python library that is able to simulate a ray-tracing of a beam to some simple optical element, such as mirror, and other a bit complicated that are basically a combination of mirrors element such as Kirkpatrick-Baez (KB) system and a Montel system.

Moreover the Montel code it is used to understand the effect of such element with respect to an incident beam in order to

The thesis is struchter in

1. Chapter 1: review of the interaction x-ray - matter in order to explain the importance of the mirror in a grazing configuration for x-ray radiation
2. Chapter 2: it is reported the theoretical explanation of mirror effect, and it is done a study of the Kirkpatrick-Baez (KB) system and Montel system, with a comparison between them.
3. Chapter 4: describes how the python library works going defining the way in which the algoritm is written
4. Chapter 5: shows the correct operation of the program testing it with respect to OASYS, software developed by Manuel Sanchez Del Rio, end a paper. Then report the analysis of Montel simulation done.

Capitolo 1

Focusing for X-rays

Image formation usually implies some form of focusing. The focusing property depend on the environment in which the radiation its surrounded. In case of the visible light the laws of about lenses and mirrors it's well-known and studied, that is similar for the electron, where the optical element are substituted with electric and magnetic fields to curve the path of them. To study the focusing property of the X-ray radiation, it have to consider the interaction that acts between the radiation and the matter. There are three phenomena that rule this interaction:

1. elastic scattering;
2. inelastic scattering;
3. absorption via photoelectric effect.

The first effect, where there is an exchange of energy, is constituted by: Thomson scattering, that it is the scattering of electromagnetic radiation by a free non relativistic charged particle [Dal16], and Rayleigh scattering, an elastic scattering between the radiation and the strogly bounded electrons that act cooperativley [Fit06]. For the elastic scattering it have to consider also the interference figure that are generated by the interaction between the incident and the scattered radiation (Bragg diffraction), with a defined phase relation. The second effect ,inelastic scattering, or Compton scattering [Uni16], that occurs when an electron lost by the atom interact with the radiation and absorb a small energy from the X-ray radiation. This scattering is an incoherent effect so there isn't any phase relation between incident and scattered radiation, moreover the atom pass to another quantum state due to the energy absorbed by the electron. The last effect, absorption via photoelectric effect, occur when an bounded electron with an atom get the necessary energy to break the bound and become free (ionization process). Figure 1.1 show the contribution for the attenuation coefficient, of the different absorption of two different material: carbon (Figure 1.1a), and carbon (1.1b).

The X-ray radiation become relevant with the spreads with the synchrotron, and the introduction of plasma sources, because, before that the X-ray source were not sufficiently intense for experiments.

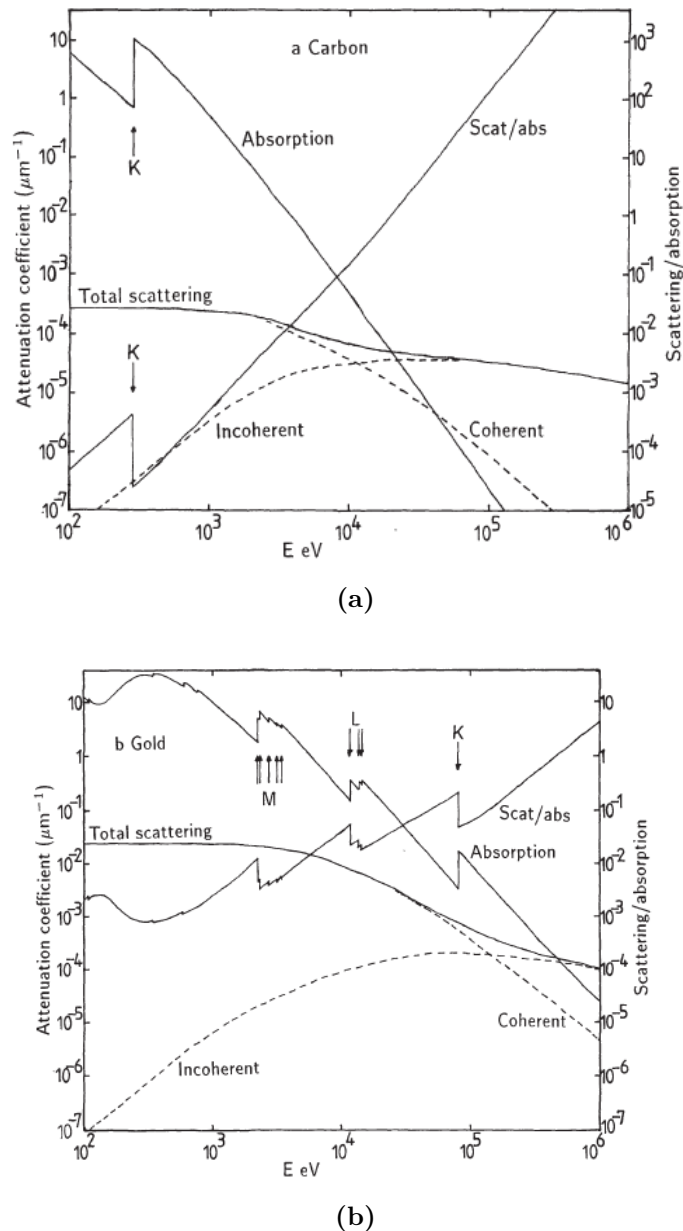


Figura 1.1: Attenuation coefficient for X-ray radiation of carbon 1.1a, and gold 1.1b

1.1 Interaction with Matter

Interaction between radiation and matter can be compressed in an coefficient (absorption coefficient)), that rule the attenuation of an incident radiation

$$I = I_0 \exp(-\alpha x) \quad (1.1)$$

where x is the thickness of the material, α is the absorption coefficient, and I_0 the initial intensity of the beam corresponding to the intensity at $x = 0$. Considering the beam as a plane wave, it is possible to express the amplitude of the electromagnetic wave as:

$$A = A_0 \exp\left(\frac{-2\pi\beta x}{\lambda}\right) \exp\left(\frac{-2\pi i(nx - ct)}{\lambda}\right) \quad (1.2)$$

where x is the position of the front wave, λ correspond to the wavelength of the wave in the vacuum, n is a number that correspond to the refractive index and depends from the material, and β in this case, correspond to the absorption coefficient of the material. The propagation of the radiation depend from the complex refractive index n , that can be expressed as:

$$\bar{n} = n - i\beta \quad (1.3)$$

For X-rays process , the absorption term is the leading term, this mean that the α coefficient can be defined as linearly dependent from the absorption coefficient, where:

$$\alpha = \frac{4\pi\beta}{\lambda} \quad (1.4)$$

As it is reported in Appendix A, the absorption values tabulated are given are the mass absorption coefficients μ , where

$$\alpha = \mu\rho \quad (1.5)$$

where ρ is the density of the material. The mass absorption of a compound is given by

$$\mu_{\text{com}} = \sum_j w_j \mu_j \quad (1.6)$$

where μ_j is the mass absorption of a particular element (the ones reported in Appendix A, and w_j is the fraction of the j element in the material. The relation between the absorption coefficient of the material and the mass absorption coefficient is:

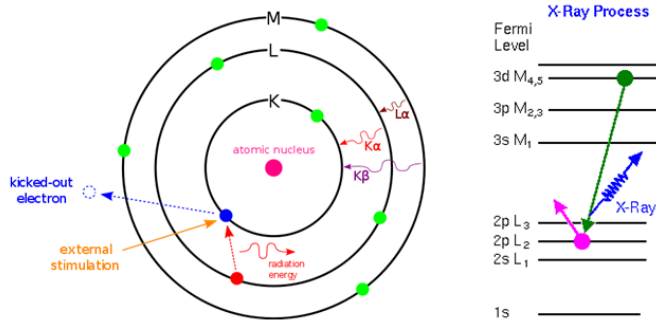


Figura 1.2: X-ray ionizing process

$$\alpha_{\text{com}} = \mu_{\text{com}} \rho_{\text{com}} \quad (1.7)$$

where ρ_{com} is the density of the compound.

Because of the dominant energy of the radiation with respect to the matter energies involved in the interaction (X-rays energies spreads from 100eV, soft X-ray, to 10keV, hard X-ray, binding and molecular energies are of the order of few eV), the ionization process is the leading process in the absorption coefficient. In this case the greater part of the energies involved is transferred to the kinetic term of the ionized electrons. Electron in atom have a well-defined state of energies, so, to be absorbed, the radiation must have the correct value of the electron state energies, the absorption edges in Figure 1.1, correspond to the binding energies of the different electron states. Figure 1.2 show the ionizing process of an X-ray photon, and show qualitatively the different energies of an outer electron with respect to the ionized one. In reality, the edges, are less pronunciation as the ones in figure, due to the finite energy width of the states, and because of the environment effect. To understand better the absorption of the X-ray radiation it is reported a brief theoretical treatment of the interaction, because the result are useful for the design of the optical element used for X-rays. The calculation start from the elastic scattering between X-ray photon against free electron (Thomson scattering). The electro-magnetic radiation is characterized by an electric field with amplitude A_0 that accelerate a free electron (of charge e and mass m_e) by an amount of $A_0(e/m)$. A charged particle that is accelerated emits radiation, this change the value of the amplitude of the electric field equal to: Accelerated charges radiate, the amplitude of the electric vector at a distance r from the charge being

$$A_T(\Phi) = \frac{e}{4\pi\epsilon_0 c^2 r} a \sin \Phi \quad (1.8)$$

where r is the distance between the electric field and the electron, Φ correspond to the angle between the position vector \mathbf{r} and acceleration vector \mathbf{a} of the electron. So, replacing a with $A_0(e/m)$:

$$A_T(\Phi) = A_0 \frac{e^2}{4\pi\epsilon_0 c^2 r} \sin \Phi \quad (1.9)$$

The second step is to go further the Thomson scattering, considering the electron bounded with the atoms. For this purpose the Thomson amplitude $A_T(\Phi)$ is multiplied to a complex number defined as a complex atomic scattering $f = f_1 + if_2$. Thus:

$$A(\Phi, E) = A_t(\Phi) * f(E) = A_T(\Phi)[f_1(E) + if_2(E)] \quad (1.10)$$

where the two function f_1 and f_2 , depend on the energy of the incident X-ray radiation that, to a first approximation, are independent from the angle between the incident and the scattered radiation ϑ . This approximation has sense because the typical radiation length ($\sim 0.1 - 10\text{nm}$) is much larger than the typical length of the atomic electronic distribution ($\sim 1 - 50\text{pm}$), the consequence of this approximation is the possibility to consider a phase scattering of the atomic wave function. The values of the two function f_1 and f_2 are calculated in the relativistic quantum dispersion theory and are given by:

$$f_1(E) = Z + 4\frac{\varepsilon_0 m_e c}{h e^2} \int_0^{+\infty} \frac{W^2 \sigma(W)}{E^2 - W^2} dW - \Delta_{rel} \quad (1.11)$$

and

$$f_2(E) = 2\frac{\varepsilon_0 m_e c}{h} E \sigma(E) \quad (1.12)$$

In Equation 1.11, the first term correspond to the Thomson scattering, where Z correspond to the atomic number of the atom. To add the angle-dependence of the scattering it is used the factor:

$$f_0 = \int_0^{+\infty} U(r) \operatorname{sinc} \left[\frac{4\pi r}{\lambda} \sin \frac{\vartheta}{2} \right] dr \quad (1.13)$$

where $U(r)$ represent the radical charge distribution and $\operatorname{sinc}(x)$ is the cardinal sine function $= \frac{\sin x}{x}$. Considering a wavelength λ of the order of nanometres, if $\sin \frac{\vartheta}{2} \leq \frac{\lambda}{2}$, $f_0 = Z$, otherwise for $\sin \frac{\vartheta}{2} = \lambda$, typically, for most element $f_0 \simeq 0.9Z$.

In Equation 1.11, the second term (the anomalous dispersion integral), represent the oscillation of the electron after the interaction with the radiation, this can be obtained treating the semi-classically the problem. This approach neglect the damping, so, near the absorption edges f_1 is inaccurate. The second term of the Equation 1.11, and in Equation 1.12 contain σ that is the photo ionization cross section expressed in $\text{m}^2 \text{atom}^{-1}$), a coefficient that is related to the mass absorption coefficient in this way:

$$\sigma(E) = A \frac{\mu}{N_0} \quad (1.14)$$

where A is the atomic weight and N_0 the Avogadro's number $N_0 = 6.22 * 10^{23} \text{ particle} * \text{mol}^{-1}$. The value of $\sigma(E)$ is theoretically obtained knowing the atomic wave function of the atom, so, only for hydrogen it is possible to have the correct value, for all the other systems, the calculation can be done with approximation methods that give some uncertainty on $\sigma(E)$, consequently on the value of f_1 and f_2 .

In Equation 1.11 the third term takes into account the relativistic effect. This correction is given by:

$$\Delta_{\text{rel}} = \frac{5}{3} \frac{|E_{\text{tot}}|}{m_e c^2} + \frac{Z}{2} \left(\frac{E}{m_e c^2} \right)^2 \quad (1.15)$$

where $|E_{\text{tot}}|$ is the modulus of the total energy of the atom (that is negative), moreover, this third term is the less relevant in Equation 1.11, for X-ray energies, so it is possible to neglect it in the calculation.

For photo absorption event by an electron bounded to an atom, far from the absorption edges, a good approximation is to consider the solid state environment distorted by the ionization of the electrons, because, the most affected electrons are the outer ones. After long calculation, is possible to relate the factors f_1 and f_2 with the macroscopic parameters n and β :

$$\delta = 1 - n = \frac{e^2 \hbar^2}{2 \varepsilon_0 m_e E^2} \overline{f}_1 \quad (1.16)$$

and

$$\beta = \frac{e^2 \hbar^2}{2 \varepsilon_0 m_e E^2} \overline{f}_2 \quad (1.17)$$

where \overline{f}_1 and \overline{f}_2 are defined as follows:

$$\overline{f}_1 = \sum_j N_j f_{1j} \quad \overline{f}_2 = \sum_j N_j f_{2j} \quad (1.18)$$

and represent the average scattering factor per unit volume, N_j is the total number of the particular j element per unit volume. Putting everything together Equation 1.16, apart near the absorption edges, can be expressed as:

$$\delta = \frac{N e^2 \hbar^2}{2 \varepsilon_0 E^2} = \frac{N e^2 \lambda^2}{8 \pi^2 \varepsilon_0 m_e c^2} \quad (1.19)$$

where N is the number of electrons per unit volume. For X-ray energies the value of δ is small (typically $\sim 10^{-3}$) and positive, this is important because it means that, for X-rays, the refractive index is a bit less than 1. It is possible to find the tabulated values of f_1 and f_2 , [?], that are the main ingredient to calculate the curve in Figure 1.1 and these were used to generate Figure 1. These values, according with the experimental results, allow to write, far from absorption edges, the absorption coefficient β such as:

$$\beta \sim Z^2 \lambda^3 \quad (1.20)$$

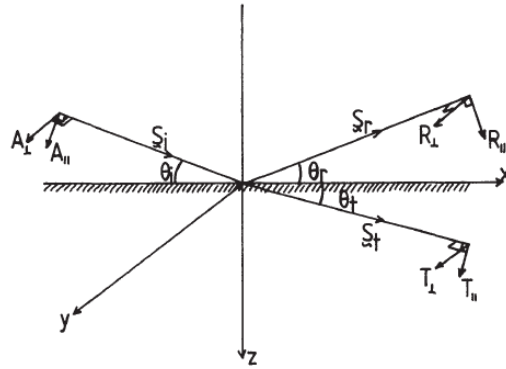


Figura 1.3: Interface of two medium

1.2 Total External Reflection

For the system in Figure 3.15, there are two complex refractive index:

$$\bar{n}_1 = 1 - \delta_1 - i\beta_1 \quad (1.21)$$

and

$$\bar{n}_2 = 1 - \delta_2 - i\beta_2 \quad (1.22)$$

moreover $\delta_2 > \delta_1$. In the general case there are, as shown in Figure 3.15 a reflected and a transmitted wave. For the theoretical treatment, initially, will be neglect the absorption ($\beta_1 = \beta_2 = 0$), moreover the permeability coefficient it is supposed to be similar to the permeability in the vacuum. Thus, the law of Snell, can be expressed such as:

$$\frac{\cos \vartheta_i}{\cos \vartheta_t} = \frac{1 - \delta_2}{1 - \delta_1} \quad (1.23)$$

Using the frame system as in Figure 3.15, with the z-axis that correspond to the normal of the interface. It is possible to write the component of the electric field of the waves in this way

$$E_{ix} = A_{\parallel} \sin \vartheta_i \exp^{-i\tau_i}, \quad E_{iy} = A_{\perp} \exp^{-i\tau_i}, \quad E_{iz} = A_{\parallel} \cos \vartheta_i \exp^{-i\tau_i} \quad (1.24a)$$

$$E_{tx} = -T_{\parallel} \sin \vartheta_t \exp^{-i\tau_t}, \quad E_{ty} = T_{\perp} \exp^{-i\tau_t}, \quad E_{tz} = T_{\parallel} \cos \vartheta_t \exp^{-i\tau_t} \quad (1.24b)$$

$$E_{rx} = R_{\parallel} \sin \vartheta_r \exp^{-i\tau_r}, \quad E_{ry} = R_{\perp} \exp^{-i\tau_r}, \quad E_{rz} = R_{\parallel} \cos \vartheta_r \exp^{-i\tau_r} \quad (1.24c)$$

where

$$\tau_i = \omega(t - \frac{\mathbf{r} \bullet \mathbf{s}_i}{v_1}) = \omega \left[t - \frac{(1 - \delta_1)(x \cos \vartheta_i + z \sin \vartheta_i)}{c} \right] \quad (1.25a)$$

$$\tau_t = \omega(t - \frac{\mathbf{r} \bullet \mathbf{s}_t}{v_2}) = \omega \left[t - \frac{(1 - \delta_2)(x \cos \vartheta_t + z \sin \vartheta_t)}{c} \right] \quad (1.25b)$$

$$\tau_r = \omega(t - \frac{\mathbf{r} \bullet \mathbf{s}_r}{v_1}) = \omega \left[t - \frac{(1 - \delta_1)(x \cos \vartheta_r + z \sin \vartheta_r)}{c} \right] \quad (1.25c)$$

where ω is the angular frequency of the wave, and v_1, v_2 , correspond to the velocities of propagation that depend on the material as follow:

$$v_1 = \frac{c}{1 - \delta_1}, \quad v_2 = \frac{c}{1 - \delta_2} \quad (1.26)$$

the related magnetic field are:

$$\begin{aligned} H_{ix} &= -A_\perp(1 - \delta_1) \sin \vartheta_i \exp^{-i\tau_i}, & H_{iy} &= -A_\parallel(1 - \delta_1) \exp^{-i\tau_i}, \\ H_{iz} &= A_\perp(1 - \delta_1) \cos \vartheta_i \exp^{-i\tau_i} \end{aligned} \quad (1.27a)$$

$$\begin{aligned} H_{tx} &= -T_\perp(1 - \delta_2) \sin \vartheta_t \exp^{-i\tau_t}, & H_{ty} &= -T_\parallel(1 - \delta_2) \exp^{-i\tau_t}, \\ H_{tz} &= T_\perp(1 - \delta_2) \cos \vartheta_t \exp^{-i\tau_t} \end{aligned} \quad (1.27b)$$

$$\begin{aligned} H_{rx} &= -R_\perp(1 - \delta_1) \sin \vartheta_r \exp^{-i\tau_r}, & H_{ry} &= -R_\parallel(1 - \delta_1) \exp^{-i\tau_r}, \\ H_{rz} &= R_\perp(1 - \delta_1) \cos \vartheta_r \exp^{-i\tau_r} \end{aligned} \quad (1.27c)$$

the boundary condition impose the continuity of the fields:

$$E_{ix} + E_{rx} = E_{tx}, \quad E_{iy} + E_{ry} = E_{ty} \quad (1.28)$$

and

$$H_{ix} + H_{rx} = H_{tx}, \quad H_{iy} + H_{ry} = H_{ty} \quad (1.29)$$

because of Snell's laws $\vartheta_r = \vartheta_t$, so, from the Equation 1.28 and Equation 1.29:

$$(A_\parallel - R_\parallel) \sin \vartheta_i = T_\parallel \sin_t \quad (1.30a)$$

$$A_\perp + R_\perp = T_\perp \quad (1.30b)$$

$$(1 - \delta_1)(A_\perp - R_\perp) \sin \vartheta_i = (1 - \delta_2)T_\perp \sin \vartheta_t \quad (1.30c)$$

$$(1 - \delta_1)(A_\parallel + R_\parallel) = (1 - \delta_2)T_\parallel \quad (1.30d)$$

Equations 1.30 give a set of equations where the parallel and perpendicular component of the waves are independent. Solving that set with respect to each parallel/perpendicular component it is obtained:

$$\frac{R_\parallel}{A_\parallel} = \left[\frac{(1 - \delta_2) \sin \vartheta_i - (1 - \delta_1) \sin \vartheta_t}{(1 - \delta_2) \sin \vartheta_i} + (1 - \delta_1) \sin \vartheta_t \right] \quad (1.31a)$$

$$\frac{R_\perp}{A_\perp} = \left[\frac{(1 - \delta_1) \sin \vartheta_i - (1 - \delta_2) \sin \vartheta_t}{(1 - \delta_1) \sin \vartheta_i} + (1 - \delta_2) \sin \vartheta_t \right] \quad (1.31b)$$

$$\frac{T_\parallel}{A_\parallel} = \frac{2(1 - \delta_1) \sin \vartheta_i}{(1 - \delta_2) \sin \vartheta_i + (1 - \delta_1) \sin \vartheta_t} \quad (1.31c)$$

$$\frac{T_\perp}{A_\perp} = \frac{2(1 - \delta_1) \sin \vartheta_i}{(1 - \delta_1) \sin \vartheta_i + (1 - \delta_2) \sin \vartheta_t} \quad (1.31d)$$

Equations 1.31 are the Fresnel formula for reflection at a plane surface. Combining them with Equation 1.23 it is obtained:

$$\frac{R_{\parallel}}{A_{\parallel}} = \frac{(1 - \delta_2)^2 \sin \vartheta_i - (1 - \delta_1) \sqrt{(1 - \delta_2)^2 - (1 - \delta_1)^2 \cos^2 \vartheta_i}}{(1 - \delta_2)^2 \sin \vartheta_i + (1 - \delta_1) \sqrt{(1 - \delta_2)^2 - (1 - \delta_1)^2 \cos^2 \vartheta_i}} \quad (1.32a)$$

$$\frac{R_{\perp}}{A_{\perp}} = \frac{(1 - \delta_1)^2 \sin \vartheta_i - \sqrt{(1 - \delta_2)^2 - (1 - \delta_1)^2 \cos^2 \vartheta_i}}{(1 - \delta_1)^2 \sin \vartheta_i + \sqrt{(1 - \delta_2)^2 - (1 - \delta_1)^2 \cos^2 \vartheta_i}} \quad (1.32b)$$

$$\frac{T_{\parallel}}{A_{\parallel}} = \frac{2(1 - \delta_1)(1 - \delta_2) \sin \vartheta_i}{(1 - \delta_2)^2 \sin \vartheta_i + (1 - \delta_2) \sqrt{(1 - \delta_2)^2 - (1 - \delta_1)^2 \cos^2 \vartheta_i}} \quad (1.32c)$$

$$\frac{T_{\perp}}{A_{\perp}} = \frac{2(1 - \delta_1) \sin \vartheta_i}{(1 - \delta_1) \sin \vartheta_i + \sqrt{(1 - \delta_2)^2 - (1 - \delta_1)^2 \cos^2 \vartheta_i}} \quad (1.32d)$$

When ϑ_i is such that:

$$\cos \vartheta_i = \frac{1 - \delta_2}{1 - \delta_1} \quad (1.33)$$

that angle is named critical angle ϑ_c , and

$$\frac{R_{\parallel}}{A_{\parallel}} = \frac{R_{\perp}}{A_{\perp}} \quad (1.34)$$

this case correspond to a wave that is totally reflected. Normally the total external reflection take place at an interface light material(air/vacuum) and dense material, so $\delta_1 = 0, \delta_2 = \delta$, the equations became:

$$\frac{R_{\parallel}}{A_{\parallel}} = \frac{(1 - \delta)^2 \sin \vartheta_i - \sqrt{(1 - \delta)^2 - \cos^2 \vartheta_i}}{(1 - \delta)^2 \sin \vartheta_i + \sqrt{(1 - \delta)^2 - \cos^2 \vartheta_i}} \quad (1.35a)$$

$$\frac{R_{\perp}}{A_{\perp}} = \frac{\sin \vartheta_i - \sqrt{(1 - \delta)^2 - (1 - \cos^2 \vartheta_i)}}{\sin \vartheta_i + \sqrt{(1 - \delta)^2 - \cos^2 \vartheta_i}} \quad (1.35b)$$

$$\frac{T_{\parallel}}{A_{\parallel}} = \frac{2(1 - \delta) \sin \vartheta_i}{(1 - \delta)^2 \sin \vartheta_i + \sqrt{(1 - \delta)^2 - (1 - \cos^2 \vartheta_i)}} \quad (1.35c)$$

$$\frac{T_{\perp}}{A_{\perp}} = \frac{2 \sin \vartheta_i}{\sin \vartheta_i + \sqrt{(1 - \delta)^2 - \cos^2 \vartheta_i}} \quad (1.35d)$$

introducing the absorbing coefficient $\beta_2 = \beta \neq 0$:

$$\frac{R_{\parallel}}{A_{\parallel}} = \frac{\bar{n}^2 \sin \vartheta_i - \sqrt{\bar{n}^2 - \cos^2 \vartheta_i}}{\bar{n}^2 \sin \vartheta_i + \sqrt{\bar{n}^2 - \cos^2 \vartheta_i}} \quad (1.36a)$$

$$\frac{R_{\perp}}{A_{\perp}} = \frac{\sin \vartheta_i - \sqrt{\bar{n}^2 - \cos^2 \vartheta_i}}{(\sin \vartheta_i + \sqrt{\bar{n}^2 - \cos^2 \vartheta_i})} \quad (1.36b)$$

$$\frac{T_{\parallel}}{A_{\parallel}} = \frac{2\bar{n} \sin \vartheta_i}{\bar{n}^2 \sin \vartheta_i + \sqrt{\bar{n}^2 - \cos^2 \vartheta_i}} \quad (1.36c)$$

$$\frac{T_{\perp}}{A_{\perp}} = \frac{2 \sin \vartheta_i}{\sin \vartheta_i + \sqrt{n^2 - \cos^2 \vartheta_i}} \quad (1.36d)$$

For interface that are curved, the Equations 1.36 are still valid if the curvature radius is much grater than the wavelength, condition that is satisfied for the X-ray radiation. Let's define the two reflectivity:

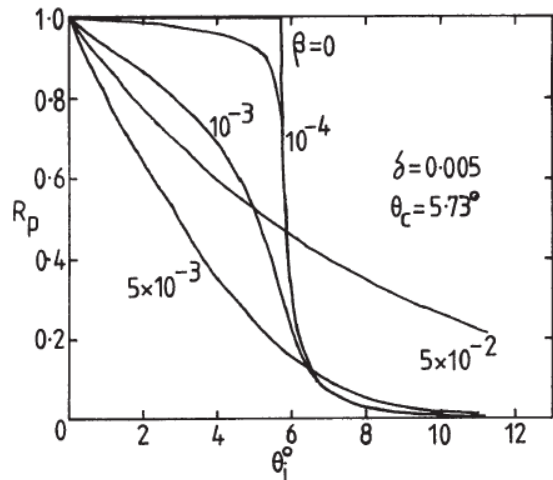
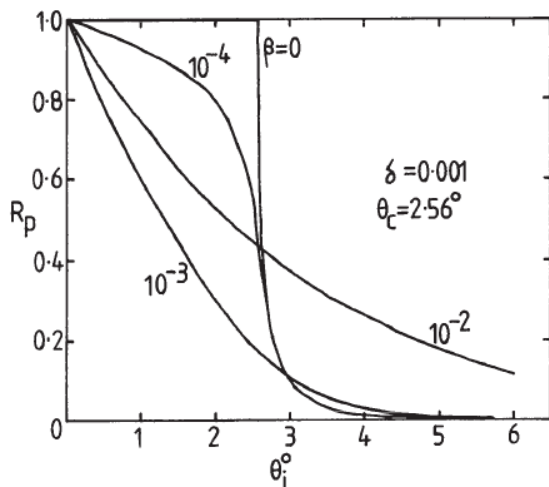
$$R_p = \frac{R_{\parallel}}{A_{\parallel}} \left(\frac{R_{\parallel}}{A_{\parallel}} \right)^* \quad (1.37)$$

and

$$R_p = \frac{R_{\parallel}}{A_{\parallel}} \left(\frac{R_{\parallel}}{A_{\parallel}} \right)^* \quad (1.38)$$

Figure 1.4 show the trend of R_p for two different δ (Figure 1.4a $\delta = 0.005$, Figure 1.4b $\delta = 0.001$), changing the absorption coefficient β . It is possible to note that R_p have a big values for small β for small grazing incidence angles, minor than the critical angle, beyond the critical angle, R_p decrease quickly to zero. On the contrary, for big values of β , R_p decrease gradually before and after the critical angle. The situation of R_s , in case of small angle, is similar $R_s \simeq R_p$ as it is showed in Figure 1.5, where it is plotted the ratio $\frac{R_s}{R_p}$ with respect to the incidence angle. As it is shownen, for small angle, the two values are similar, increasing the angle the situation differ, but, in this case, the values of R_s and R_p is very small as it is showed in Figure 1.6. In reality β is never zero so it is not possible to have a total external reflection, it is convenient to define that the total external reflection occurs when the curve reflectivity with respect to the incidence angle have a point of inflection. Figure 1.7 show that the condition it is satisfied when:

$$\beta < 0.63\delta \quad (1.39)$$

(a) $\delta = 0.005$ (b) $\delta = 0.001$ **Figura 1.4:** R_p 's values for grazing incidence with two values of δ , and some values of β

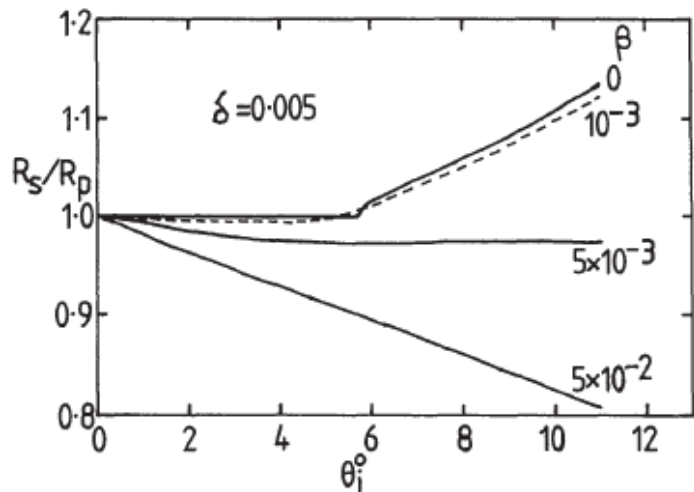
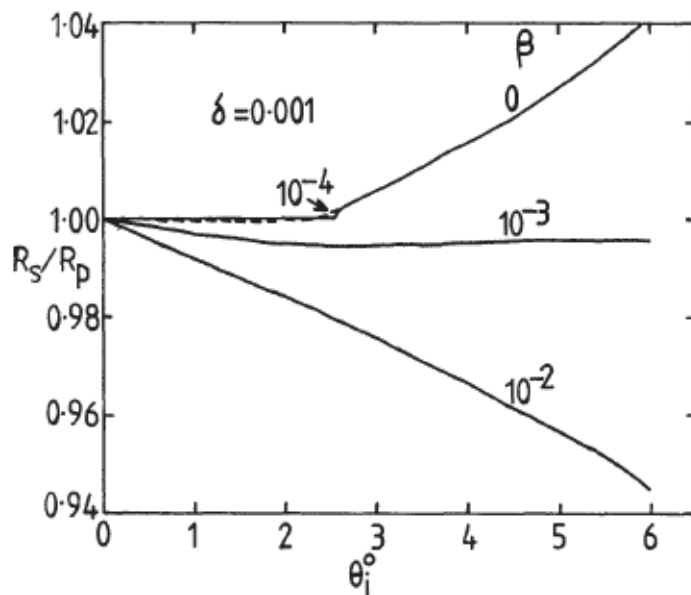
(a) $\delta = 0.005$ (b) $\delta = 0.001$

Figura 1.5: Ratio of $\frac{R_s}{R_p}$ for two values of δ , and some values of β

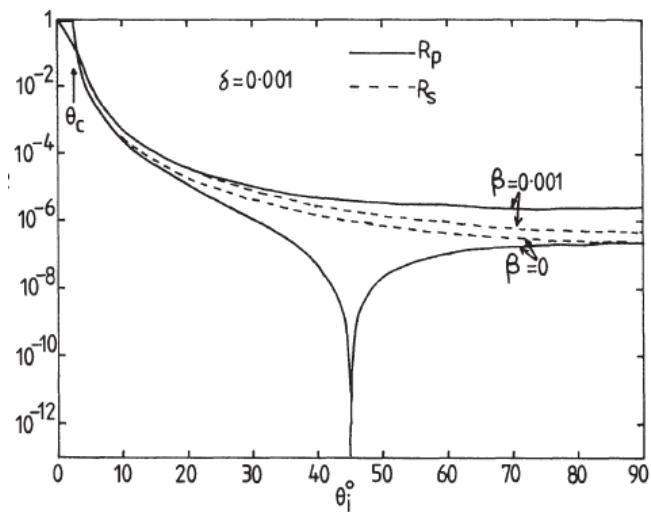


Figura 1.6: Reflectivity over the whole values of incidence angles

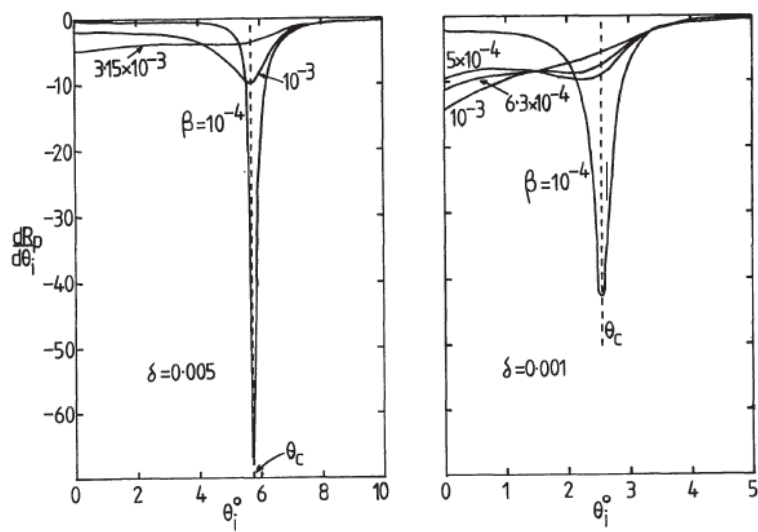


Figura 1.7: Slopes of reflectivity which show that, to have an inflection point, $\beta < 0.69\delta$

Capitolo 2

Mirrors for X-rays

“Terence: Tu lo reggi il whisky?

Bud: Beh, i primi due galloni si, al terzo divento nostalgico e ci può scappare la lite... E tu lo reggi?

Terence: Eh, che domande, io sono stato allattato a whisky!”

I due superpiedi quasi piatti

As discussed in Chapter ??, to have focusing properties for X-ray radiation, refraction optics are useless, due to the strong interaction with matter of X-rays. Thus reflection optics, at grazing incidence angle to have a good signal is needed. Mirrors that carry out any focusing must have a curved surface. A Working at normal incidence, it is possible to obtain a form a good image using a concave mirror. But this is not the case for X-ray that work, as said before, at grazing angle, this introduce some kind of optical aberration. A spherical surface has the property that the rate of change of the surface slope is exactly the same everywhere on the surface, and thus the aberration is inevitable. This shape bring an intrinsic aberration ("spherical aberration"). If the slope is not any more constant all over the mirror but become flatten in the region surrounding the outer rays, it is possible to focus all the rays in the same point. While correction of spherical aberration is not the only application of aspherical surfaces, it is one of the major application areas.

2.1 Spherical surface

To define a spherical surface is needed only the radius of curvature. A spherical surface is defined by only one parameter, the radius of curvature of the surface.

2.1.1 Astigmatism

In Figure 2.1 it is showd an image formation of a beam with a spherical mirror with radius R , at grazing incidence ϑ_i , with a divergence β from the point source P. The object length u is equal to the distance PO and the image distance v correspond to OQ. The beam hit the mirror over a distance equal to $k = NO$, such as $k \ll R$, that correspond to a small divergence β . The cord NO subtends an angle α with

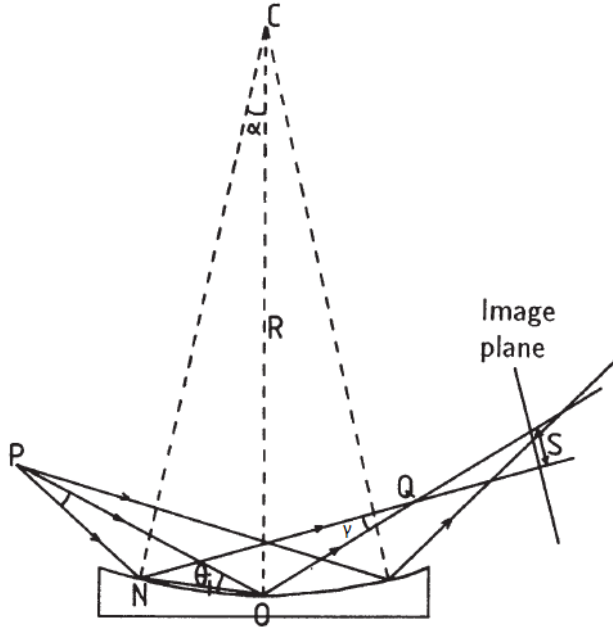


Figura 2.1: Formation image of a circular mirror

the center of the sphere C, thus $k = R\alpha$, γ is the convergence angle of the beam at the focal point Q. For small angle approximation, from the triangle PNO ,

$$\beta = R\alpha \frac{\vartheta_i - \alpha/2}{u - R\alpha} \quad (2.1)$$

and from QNO

$$\gamma = R\alpha \frac{\vartheta_i + \alpha/2}{v + R\alpha} \quad (2.2)$$

The reflection law impose that $\beta + \gamma = 2\alpha$, thus:

$$\frac{1 - \alpha/(2\vartheta_i)}{u - R\alpha} + \frac{1 + \alpha/(2\vartheta_i)}{v + R\alpha} = \frac{2}{R\vartheta_i} \quad (2.3)$$

in case of paraxial approximation

$$\frac{1}{u} + \frac{1}{v} = \frac{2}{R\vartheta_i} = \frac{1}{f_m} \quad (2.4)$$

where

$$f_m = \frac{R \sin \vartheta_i}{2} \quad (2.5)$$

that it reduce to $f_m = \frac{R\vartheta_i}{2}$ for small angle, f_m is named meridian focal length.

In case of a three dimensional spherical mirror, a second image is generated, as it is showed if Figure 2.2,with a focal distance equal to:

$$f_s = \frac{R}{2 \sin \vartheta_i} \quad (2.6)$$

and it is named sagittal focal length. For Figure 2.2 it is possible to note that the

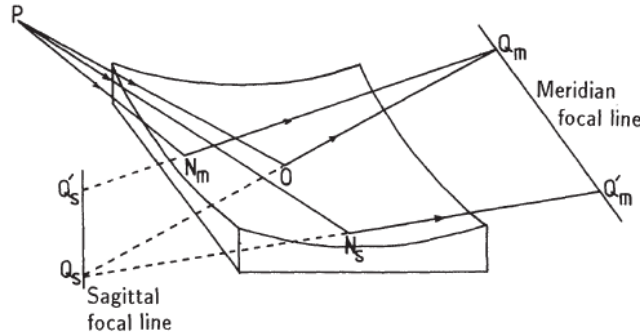


Figura 2.2: Image formation of a 3D spherical mirror

two image for a point wise source are lines, where the meridial line is in the plane of the mirror and the sagittal line perpendicular to it. Equation 2.5 and Equation 2.6, are equal for incidence angle $\vartheta_i = 0^\circ$. In the case of grazing incidence the situation is bad, for example, with a $\vartheta_i = 2^\circ$, the sagittal focal length is 10^3 times the meridial length.

2.1.2 Spherical Aberration

Spherical mirror are also affected, as it is showed in Figure 2.1, by a transverse spherical aberration. This aberration can be determined relating it with the variation of v with α :

$$S = \Delta v \sin \gamma \simeq \Delta v \gamma \quad (2.7)$$

where S is the coefficient that determine the spherical aberration. Moreover, from Equation 2.3, in case of $\alpha = 0$:

$$v_0 = \frac{f_m u}{u - f} \quad (2.8)$$

otherwise:

$$v = v_0 + \Delta v = f_m u - \frac{\frac{3uR\alpha}{4} + \frac{R^2\alpha^2}{2}}{u - \frac{3R\alpha}{4} - f_m} \quad (2.9)$$

defining a magnification such as

$$M = \frac{v}{u} \quad (2.10)$$

combining it with Equation 2.1 and Equation 2.2

$$\gamma = \frac{2\alpha}{M + 1} \quad (2.11)$$

So

$$S = \frac{3R\alpha^2}{2}(M + 1) = \frac{3k^2}{2R}(M + 1) \quad (2.12)$$

the dependance of S with respect to k is quadratic, so all the rays are deviated to the same side of $\alpha = 0$ image point.

2.1.3 Reducing aberration

For spherical mirror it is possible to reduce the aberration using large grazing angle (decrease astigmatism) and small aperture (decrease spherical aberration). For the first solution it have to consider the total external reflection, so it have to choose a material that have a big value of the critical angle ϑ_c . An example can be the Carbon that have a critical angle of $\vartheta_c = 18^\circ$ for K_α radiation, this correspond to have a ratio f_s over f_m of 11, that is still big.

Reducing the aperture it means to reduce k , it is reduce also the spherical aberration but also the collecting power of the mirror. This is bad because the resolving power is limited by the diffraction limit that is $\simeq \frac{\lambda}{2\vartheta}$, where ϑ is the maximum semiaperature, that, for grazing angle, correspond to ϑ_i .

2.2 Conic Surfaces

As said before, to go beyond the spherical mirror correcting the aberration, there exist aspherical surfaces that are defined with more than one parameter, in general by an analytical formula. The easier aspherical surface is the toroidal surface, a surface that is defined with two radii of curvature, the meridian one R_m and the sagittal one R_s . A particular choice of radii can be

$$R_m \sin \vartheta_i = \frac{R_s}{\vartheta_i} \quad (2.13)$$

in such a way to have equal focal length and so no asygtmatism. Thus

$$R_s = R_m \sin^2 \vartheta_i \quad (2.14)$$

Other kind of aspherical surfaces are those named "*conicsurfaces*" that can be defined as

$$z = \frac{cr^2}{1 + \sqrt{1 - (1 + k)c^2r^2}} \quad (2.15)$$

where c is the base curvature at the vertex, k is a constant that define the kind of conical surface, and r is the radial coordinate of the point on the surface. In Table 2.1, and in Figure 2.7 is showed the relation between the k constant and the kind of surface

Conic Constant k	Surface Type
0	Sphere
$k < -1$	Hyperboloid
$k = -1$	Paraboloid
$-1 < k < -0$	Ellipsoid
$k > 0$	Oblate Ellipsoid

Tabella 2.1: Parameter of different conic surfaces

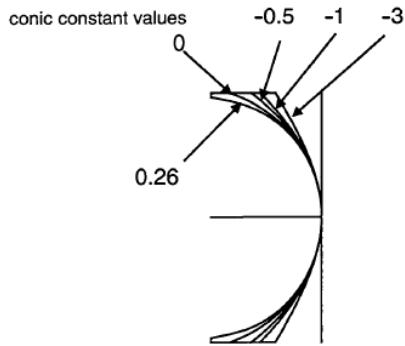


Figura 2.3: Different kind of surface conic, with the same c base curvature value, and different constant k .

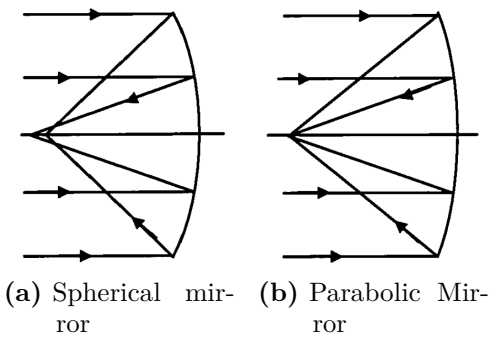


Figura 2.4: Example of spherical aberration correction

A good point that have the conical surfaces are the no-presence of spherical aberration. As said in before, spherical surface affected by spherical aberration if the configuration is different from the normal incidence. The ellipsoidal geometry forms create a free-aberration image for a couple of real object on the same side of the surface, on the contrary the hyperbola work for conjugates on different side of it. Parabolic surface create a perfect image for any axial object place at infinity, this is the reason why parabolic mirror are very used for astronomical application. For all the shapes of surfaces, if the object is moved from its ideal position aberration will appear: an axial movement introduce a certain amount of spherical aberration, lateral movement introduce other types of aberration such as coma, astigmatism and field curvature.

The importance of aspherical surface for mirror consist in the fact that, differently from the lenses, is not possible to build a spherical surface with different radii, in the lenses case it different spherical radii, and so, aspherical surface, serve to minimize the aberration. Figure 2.4 show a simple example of how it is possible to correct the spherical aberration using a paraboloid mirror 2.4b instead of a spherical mirror 2.4a

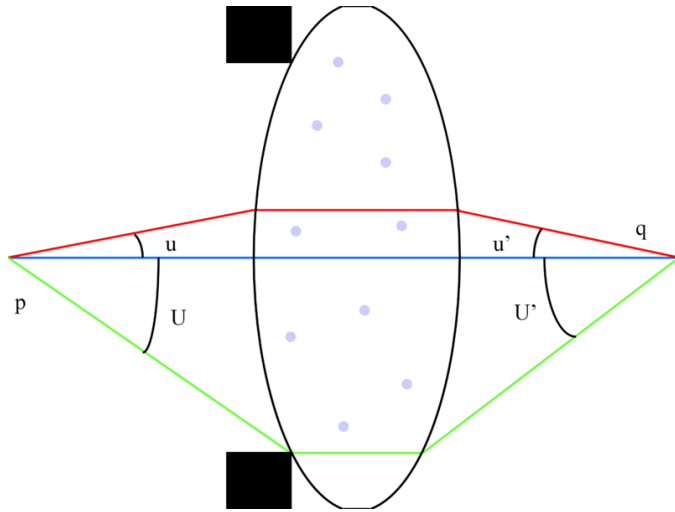


Figura 2.5: Sine Abbe condition for a lens

2.3 Compound Optical system

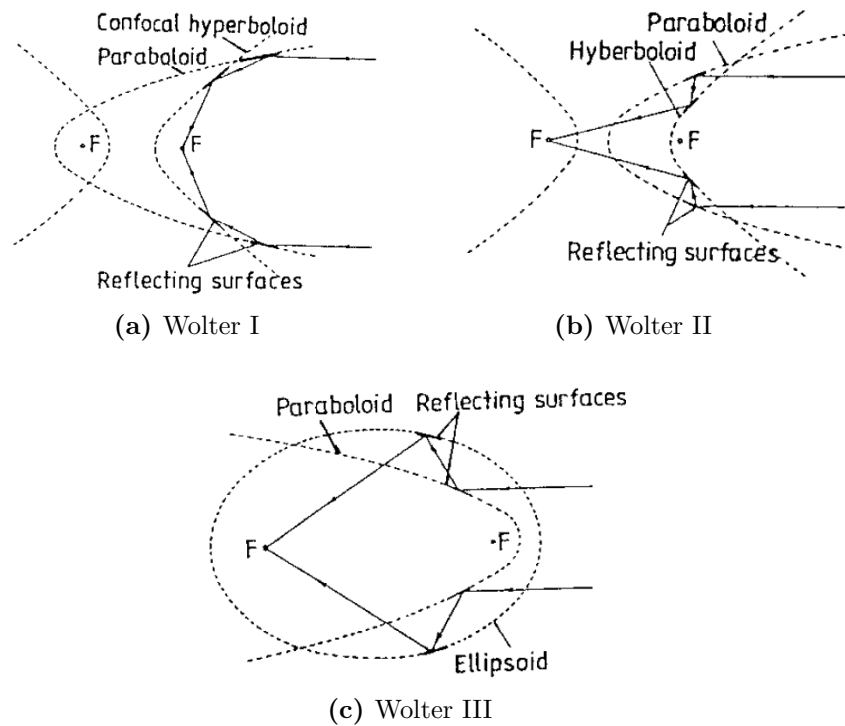
An optical system designed to obtain an image that reproduce correctly the object image must satisfy the Sine-Abbe condition

$$\frac{\sin u'}{\sin U'} = \frac{\sin u}{\sin U} \quad (2.16)$$

where, as it is showed in Figure 2.5, u and u' are rays that leave the object, U and U' are the angles of the same rays that reach the image plane. In other world, the sine of the ray that leave the object must be proportional to the sine of the angles that reach the image plane. Unfortunately, for the case of mirror, there is no way to satisfy the Sine Abbe condition using only one mirror. To satisfy the condition, and so obtain a better image, there are invented optical system composed by more than one mirror. The system that whose invented which respect the condition are the Wolter system, widely used in astronomy, that use a combination of coaxial and confocal conic section. A first approximation system that respect the sine Abbe condition are the Kirkpatrick-Baez system and Montel or nested-Kirkpatrick-Baez system, those compound optical system involves reflector whose meridian planes are at right angle (crossed).

2.3.1 Wolter System

In 1952 Wolter published a paper in which he discussed several disposition of two conical mirror in order to collect light for an astronoical use. Figure show the different disposition discussed: Wolter I, Wolter II, Wolter III. Wolter I telescope consist of a coaxialparaboloid (primary mirror) and hyperboloid (secondary mirror). The focus of the paraboloid is coincident with the rear focus of the hyperboloid, and the reflection inside both mirrors. The Wolter II telescope use the same kind of mirror of Wolter I paraboloid and hyperboloid. But the focus of the paraboloid coincident with the front focus of the hyperboloid, and, the reflection, occurs internally for the paraboloid and externally for the hyperboloid. The Wolter III



telescope consist in a paraboloid and an ellipse. In this system the first mirror is the paraboloid one, and the second is the ellipsoidal that have front focus coincident with that of the parabola, moreover the reflection is external for the paraboloid and internal for the ellipsoidal. The Wolter I have typical grazing angle of less than a degree and is used for hard X-rays. The Wolter II telescope has typical grazing angle of, approximate, 10 degree and is used for soft X rays and extreme ultraviolet (EUV). Because of circular symmetry, astigmatism and spherical aberration are eliminated but exhibit coma aberration. Other problem is the difficulty of fabrication , and require a huge area to achieve a very small collecting angle.

2.3.2 Kirkpatrick-Baez System

This kind of optics are used in the ESRF and consist, as shown in Figure, in two separated cylindrical surface conical mirror that focus the incident beam in both saggital and transverse thus astigmatism is removed. Although such system introduce another type of distortion, anamorphotism. Because of the different distance of the image plane with respect to the mirrors the magnification is different in the two direction. Another technical problem that face with system is the big volume that occurs to implement it. To overcome those two problem and obtain a system that conjugate the good behaviour of the KB system with an equal magnification of the two direction and compact system, it is possible to implement a system as it is showed in Figure, a system in which both mirrors are at the same distance from the object. This sort of arrangement is extremely difficult to manufacture and, consequently, very expensive. Despite these problem K-B system are very used in ESRF and in European synchrotron, on the contrary, in American

synchrotron another type of optical system, named "Montel", is used that will be discussed in the next section.

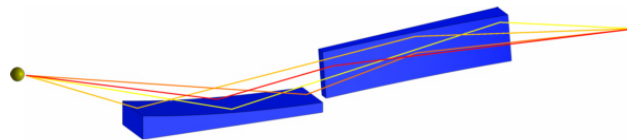


Figura 2.6: Kirkpatrick-Baez system

2.4 Montel

As discussed before KB system have some limitation that can be overcome with a different optical system named "Montel". This geometry bring four important advantages for high-precision focusing:

- i) the optical system is more compact which allow greater working space;
- ii) the focal distance of the two mirror are the same, this cancel out the anamorphotism;
- iii) the alineation of the system is easier with respect to the KB system because, in this case, only one thing has to be aligned, however , in the KB there are two separated mirror that has to be aligned;
- iv) the divergence that can be collected is larger which allows for greater flux and/or a lower diffraction limit.

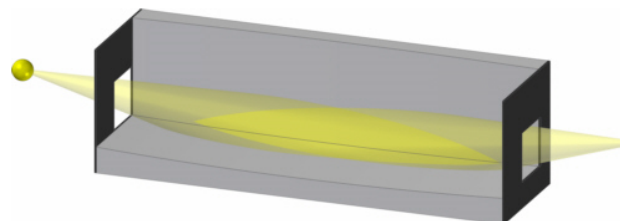


Figura 2.7: Montel system

2.4.1 Diffraction limit of Montel compared to sequential K:

The image quality and dimension, for x-rays reflective optics, is caused by aberration, mirror imperfection, and magnification of the system. Nowadays it is possible to create a mirror with high surface quality with a so high demagnification that the spot focal size is limited, primary, by diffraction and mechanical/environmental factors.

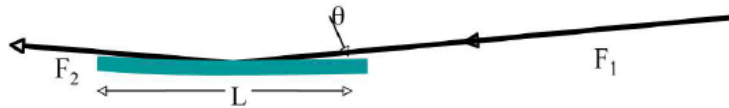


Figura 2.8: Standard parameters that define an elliptical mirror

The first limiting factor (diffraction) depends on the wavelengths of the radiation and on the divergence of the Beam. Figure 2.8 show a simple elliptical mirror with an object focal of F_1 , an image focal of F_2 , an incidence angle ϑ and a length of the mirror equal to L . For practical calculation it is convenient to use the system in Figure 2.9 , where F_d is the distance from the end of the mirror to the image focal, ϑ_i the divergence focused at the image point, ϑ_d the maximum accepted angle, ϑ_o , the divergence intercepted by the mirror.

For an elliptical KB system the FWHM of the diffraction limit in each plane is:

$$D_{FWHM} \sim \frac{0.88\lambda}{\vartheta_i} \quad (2.17)$$

where λ is the wavelength of the radiation. For the total external reflection that rules the reflection for the X-ray, the maximum divergence that can be collected is that which correspond to the critical angle ϑ_c , that can be calculated as

$$\vartheta_c \sim \sqrt{\rho\delta} = 6.710^{-2}\lambda(nm) = \frac{8.410^{-2}}{E(keV)} \quad (2.18)$$

In reality, due to geometrical constrain on sequential KB system, the maximum divergence that can be collected is about $0.84\vartheta_c$.

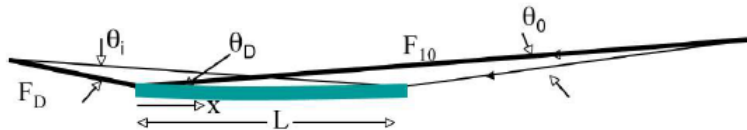


Figura 2.9: New parameter that define an elliptical mirror, useful for calculation

To study the diffraction limit of a KB system, it is done a theoretical treatment of micro focusing using elliptical mirror, and working on the parameter that define the geometrical shape, using the system in Figure 2.9. The image and objective divergence, ϑ_i and ϑ_o , depend on the angle ϑ_d , the ratio L over F_d , length of the mirror over the distance between the image focus and the end of the mirror, and the angle ϑ_d . Figure 2.10a can be used to estimate the fraction of the mirror that can reflect different wavelengths. If the mirror is designed to work for the wavelength λ with $\vartheta_d = \vartheta_c$, a new wave with wavelength equal to $\lambda/2$, the part of the mirror that is covered is that with $x/F_d > 3.5$ reflect efficiently the radiation. With Figure 2.10b it is possible to estimate the radiation collect at the image plane. Normalizing the length of the mirror with F_d and, normalizing the divergence angle collected with the biggest angle ϑ_d , then the normalized numbers fall down to a universal curve across menobhysa di a factor of 10-20. This curve is useful because it can estimate the radiation collected by the KB/Montel. For example, if L/F_d is n for

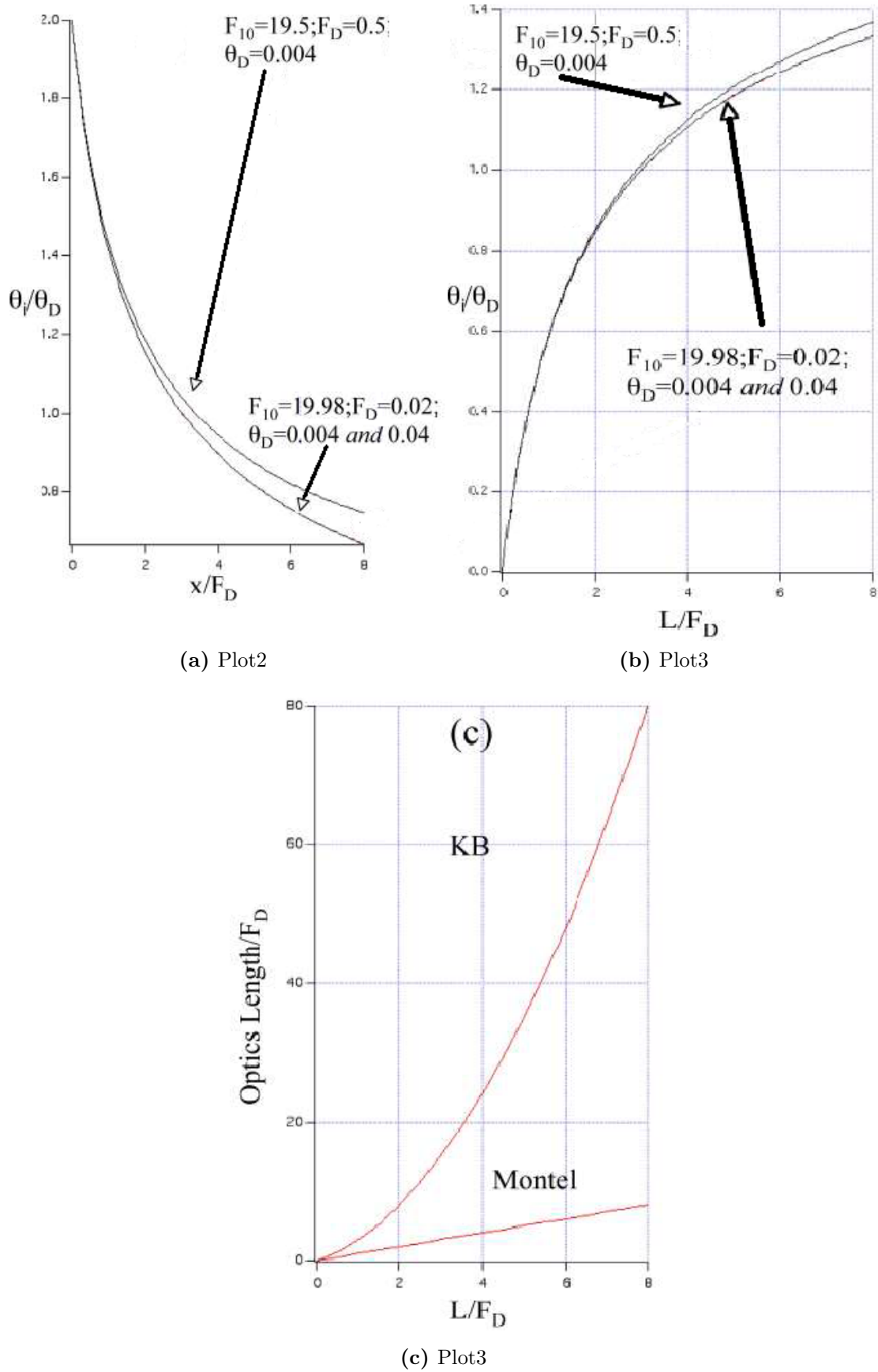


Figura 2.10: Plots

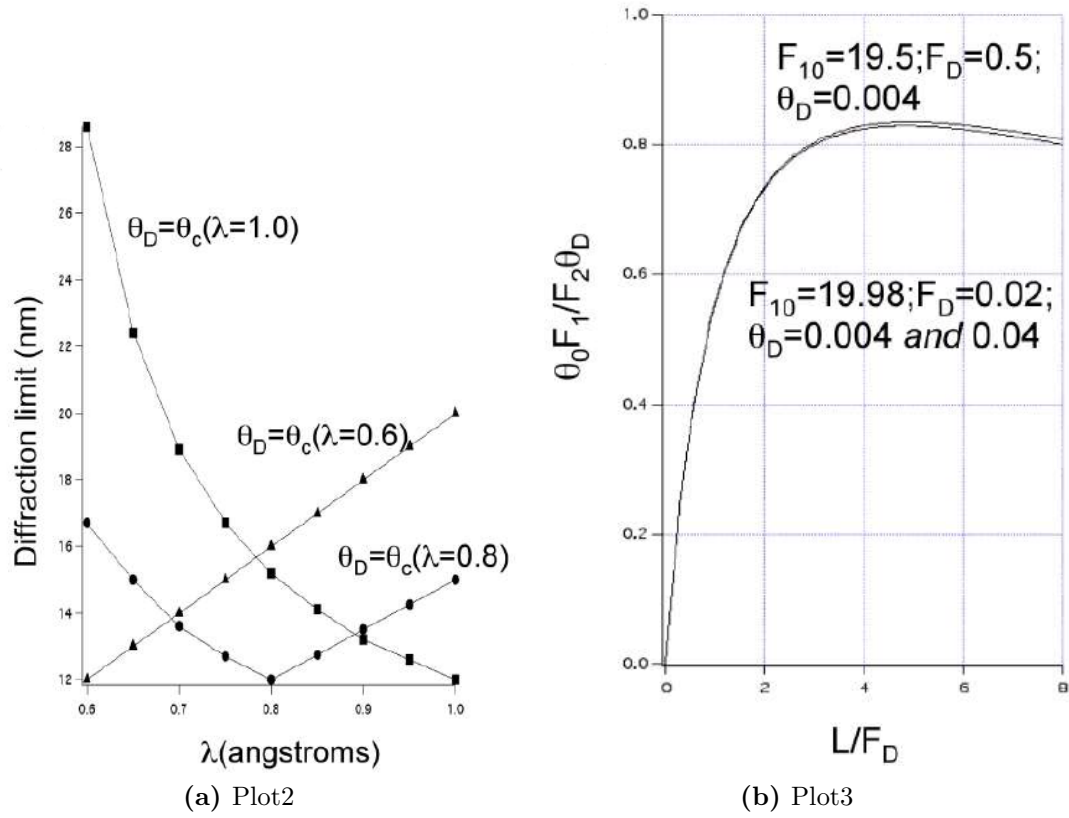


Figura 2.11: Plots

each mirror of the KB system, then the total length of the system is related to the clearance distance of the second mirror

$$L = (2n + n^2)F_d \quad (2.19)$$

for the Montel system the total length is only $L = nF_d$. In Figure 2.10c is showed the length of both compound system, and, for large $n > 2$ the situation is dramatical, for example for $n = 2$ KB length is about the same of Montel with $n = 8$. This mean that the diffraction limit for total external reflection for KB is about 16nm , for Montel 11nm .

Mirrors can be designed to work well with short or medium or large wavelengths. Depending on the design, the diffraction limit is limited to certain conditions. If the mirrors are designed for short wavelength, according to Equation 2.17, the diffraction limit is mainly governed by the wavelength, because the divergence collected is roughly independent from the wavelength. On the contrary, if the mirror are optimized to long wavelengths, the surface that reflect the radiation is only a fraction, this compromise the shortest wavelength. Figure 2.11a show the dependance of the diffraction limit with mirror designed to be optimize, with the choice of the ϑ_d to different situation.

2.4.2 Flux limit

If the beam is small, the flux is the limiting factor to the image spot. For the KB optics designed to demagnify the source, increasing the length of the mirror than the collected divergence increase, the backdraw is that the demagnification decrease, in the sense that became less strong, so, to reobtaine the desired image dimension it have to decrease the object spot. The geometrical demagnification is, according to Figure 2.9,

$$\frac{F_d(1 + n/2)}{F_1 0 - n F_d / 2} = \frac{F_2}{F_1} \quad (2.20)$$

and the collect divergence of the radiation at the image plane is ϑ_0 . As it is reported in Figure 2.11b, the performance fall down to another universal curve for large and small demagnification.

In this case the Montel system is better than the KB optics because of the larger numerical aperture that increase the flux on the sample. This last point is convenient for neutron experimental uses where the flux limit overcame the diffraction limit, differently than the X-ray experiments. Montel flux is 2.6 times increase with respect to the KB. A Montel long 0.25m of clearance has $n = 2$, a similar value to the longest of the mirror give an $n \sim 0.73$, with a difference in the total flux collect into a small spot of ~ 2.5 .

2.4.3 Optical Design

The mirrors used in this Montel configuration are mirror that have a cylindrical shape in one direction and elliptical shape in the other direction. One approach to obtain the Montel system is that to use two pre-figured elliptical mirror and grind the cut site at 45° as shown in figure. After that it place the mirrors together makes a good fit with no gap requiring no contouring of the mirror side. Another way involves diveding pre-figured elliptical mirror into two part that, add them together, can form the Montel system. This approaches is primary driven by the fact that in a conventionally polished mirror, the clear aperture area has the best figure and finish. As such uAs such, using two halves of a prefigured mirror cut in the middle has several advantages- including consistency and economy. There are major challenges however. First, the mirror surface must be protected against damage and deformation during cutting and subsequent figuring operations. After cutting into two, the cut sites must be treated (e.g., etched) to remove any subsurface damages that could alter a mirror's figure. Then the mating side of one of the mirrors must be contoured and polished such that when it is placed against the partner mirror, it makes a nearly perfect fit with good surface quality all the way to the contact edge. This last two-steps are crucial because if there is a significant gap or if the mirror surfaces in the vicinity of the interface are damaged, a significant part of the incident beam could be lost. As an example, we are developing a pair of Montel mirrors for polychromatic nanofocusing on Sector 33 at APS. This beam line will use 40 mm long elliptical mirrors for nano-focusing a 100 μm beam to a 50 nm spot at 2000x demagnification. This concave elliptical mirror has a maximum depression of about 6 μm at its center. If cut flat and placed against its mating mirror, a gap as large as 6 μm is created which loses about 10% of the 100 μm incident beam.

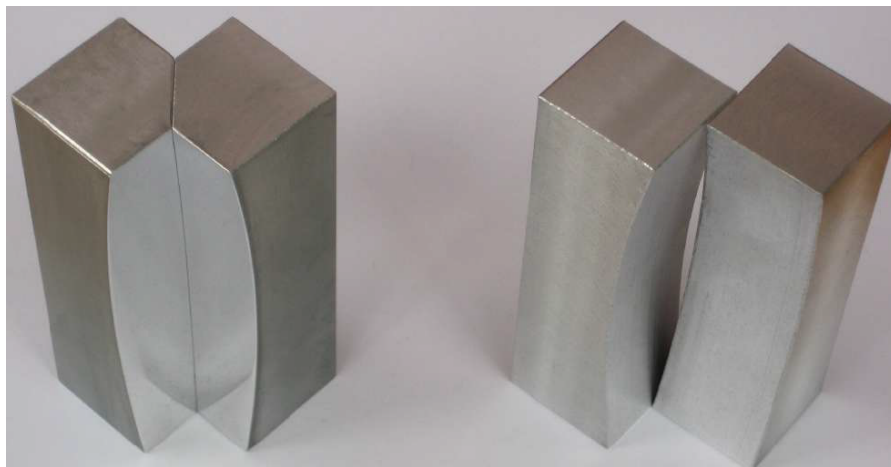


Figura 2.12: Example in how to build a Montel system starting from two cylindrical mirror cutting the edge with ad angle of 45° .

Similarly, if the mirror surfaces near the intersection are damaged, then beam loss can be significant.

Capitolo 3

MONWES

“Bud: No, calma, calma, stiamo calmi, noi siamo su un’isola deserta, e per il momento non t’ammazzo perché mi potresti servire come cibo ...”

Chi trova un amico trova un tesoro

My thesis' work is the creation of a python script that simulate a ray-tracing of a beam. This tracing take in account the effect of different type of optical elements that can find the beam in its way. To implement this ray-tracing it have to define three elements:

- Beam
- Optical elements
- Tracing system

3.1 Beam

Beam object is the object that contain the spatial and velocity information of a collection of rays. The Beam object is mainly charecterized by four parameters:

- Number of rays
- Spatial profile
- Divergence profile
- Flag vector

Starting from the begging it can say that having a large number of rays is useful in terms of results but, as a back draw, increase the computation time, so, it have to find a compromise between the number of rays and the computation time depending on the quality desired. By default, the number of rays, is setted $25 * 10^3$ that allow to have good results without spending lot of time. To change the number of rays it need to do as in figure 3.1, where, the number of rays is choose as 10^4 .

```

1   from monwes.Beam import Beam
2
3   beam = Beam(N=10**4)

```

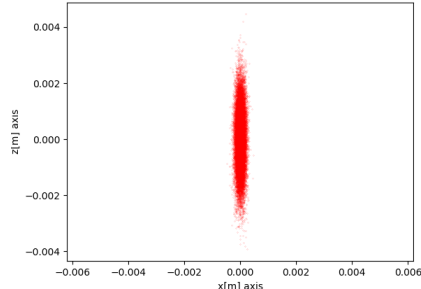
Figura 3.1: Example of Beam definition

Defined the Beam with its number of rays it have to choose the spatial and divergence profile. For the spatial profile there are some possibilities that correspond to different geometrical figure such as: rectangular profile, circular profile, Gaussian profile, point wise profile. The default one is the point wise profile, that it is useful for ideal testing, obviously, for this case, there is no input parameter. All the other profile are characterized by external input in order to define the profile depending on the nature of the profile. for the Gaussian profile the parameter needed is the σ_x and σ_z that correspond the the σ of the two dimension, Figure 3.2a show a code example to define a Gaussian spot of a Beam having $25 * 10^3$ rays with the two σ different, $\sigma_x = 0.1\text{mrad}$, $\sigma_z = 1\text{mrad}$ as it is showed in Figure 3.2b.

```

1   from monwes.Beam import Beam
2
3   beam = Beam()
4   beam.set_gaussian_spot(1e-4, 1e-3)

```

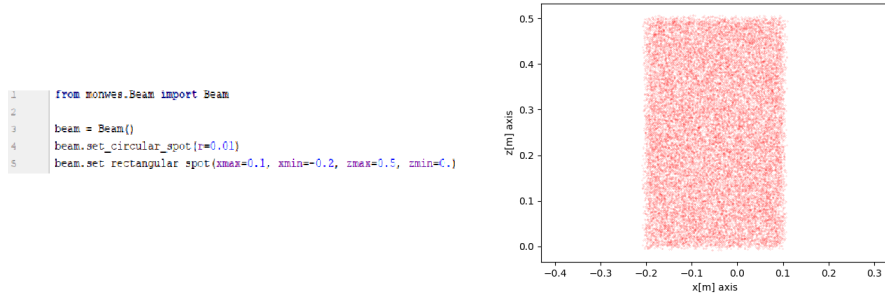


(a) Example code for a Gaussian spot

(b) Plot of Figure 3.2a

Figura 3.2: Example 1

Over the Gaussian profile, there are other two geometrical profile that can be defined rectangular and circular that have a uniform distribution, of the rays, in their space domain. For the rectangular distribution the parameter to define are the xz limit of the coordinate that define the sides of the rectangle. Figure 3.3a show an example code where it is defined a circular profile with a radius of 1cm and, after, overwritten another geometrical profile having a rectangular shape, in this case the final profile of the Beam is that figured out in Figure 3.3b, a rectangular non symmetric profile with the coordinate defined in the code in Figure 3.3a.

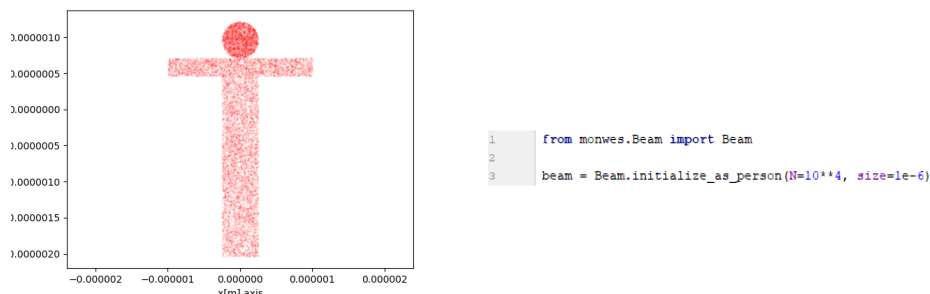


(a) Example code for a circular and a rectangular spot (b) Example plot of the rectangular profile

Figura 3.3: Example 2

Moreover it is possible to define a special shape that have, more or less, the figure of a person with a uniform distribution of the point in all the point of the space. This special shape is showed in Figure 3.4a, that is defined in the code written in Figure 3.4b. As it is showed, the initialize_as_person command take two input parameter, the number of the total rays (by default are $25 * 10^3$), and a size parameter that set the coordinate limit of the figure, more precisely. In Figure 3.4a the size correspond to 10^{-6} so the limit are:

- $x_{max} = 1\mu m$
- $x_{min} = -1\mu m$
- $z_{max} = 1\mu m$
- $z_{min} = -20\mu m$



(a) Example plot "person" profile (b) Example code for the "person" spot

Figura 3.4: Example 3

The last piece of the Beam object is the "Flag" vector. Every component of this vector have a correspondence with a certain ray and contain the information about the number of optical element that, the ray, travel until a particular moment. Moreover this value become negative when the ray doesn't hit an optical element,

in such a way to have an information where the rays were lost. Figure 3.5, resume the main parameter of the Beam object with their default values

```

8   class Beam(object):
9
10  def __init__(self,N=25000):
11
12      N = round(N)
13
14      self.x = np.zeros(N)
15      self.y = np.zeros(N)
16      self.z = np.zeros(N)
17
18      self.vx = np.ones(N) * 0.
19      self.vy = np.ones(N) * 1.
20      self.vz = np.ones(N) * 1.
21
22      self.flag = np.zeros(N)
23
24      self.N = N

```

Figura 3.5: Resume of the Beam object parameter

A part from the principal characteristic treated above, Beam object contain other option in order to manage better the utilization of it. The other option defined are reported here below:

- import_ from_ file(filename='filename'): define a Beam with a characteristic defined in a file '.h5'
- set_ point(x,y,z): move the Beam in a part of the space centred in the coordinate (x,y,z)
- initialize_ from_ arrays(x, y, z, vx, vy, vz, flag): define a Beam with the spatial value defined in the array x,y,z, the velocities' value defined in the array vx,vy,vz and the flag value defined in the array flag
- duplicate(): duplicate a Beam
- good_ beam(): define a Beam that, starting from another Beam, extract only the good rays (those that have a positive flag)
- part_ of_ beam(indices): define a Beam that, starting from another Beam, extract the ray that correspond to the position defined in the array indices
- number_ of_ good_ rays(): return the values of the good rays
- merge(beam2): merge a beam1 with another beam2, the first part of this new beam correspond to the beam1, and the second part to the beam2
- retrace(distance): this correspond to a free propagation in the space of the Beam within a distance equal to "distance"

At the end there are the command that plot the various characteristic of the beam, that contain the information for the plotted characteristic, for example plot_ xy() make a plot of the x and y coordinate of the beam, plot_ good_ xpzp() make a plot of the x-velocities and z-velocities of only the rays that have a positive flag

3.2 Optical Elements

Because, as discussed in Chapter 1, mirrors are the principal elements used in synchrotron the main optical element developed is the mirror, but it is also defined an ideal lens that is useful to simulate some particular profile for the Beam. that corresponding to this , more attention is focused on them, on the contrary , for testing uses, only one kind of lens, an ideal lens, is implemented.

3.2.1 Mirrors and lens

The different kind of mirror that are defined are:

- plane mirror
- sphere mirror
- ellipsoidal mirror
- paraboloidal mirror
- hyperboloidal mirror

All those geometrical shape are a subset of a surface conical figure. As is discussed in Chapter 2, and reported in Equation 3.1, a surface conic is defined by a series of coefficient.

$$a_0x^2 + a_1y^2 + a_2z^2 + a_3xy + a_4yz + a_5xz + a_6x + a_7y + a_8z + a_9 = 0 \quad (3.1)$$

The parameter needed to define the correct surface conic shape that define uniquely the mirror desired are:

- focal distances
- angle of incidence ϑ_g , more precisely the program use the complementary angle of ϑ_g that is $\vartheta = \frac{\pi}{2} - \vartheta_g$ (the input and output angle are in radiant)

Moreover, the surface conic, is defined in such a way to have the origin equal to the incidence point of a collimated ray distant p (that correspond to the object focal distance) from the mirror, and with the normal of the surface corresponding to the z-axis, as it is showed in Figure 3.8. For the plane mirror the situation is simple, because the equation of the surface is that in Equation 3.2, that have all the coefficient equal to 0 apart from a_8 that is equal to 1.

$$z = 0 \quad (3.2)$$

For the spherical case, the parameter that characterize a sphere is the radius, one time defined the radius, the equation of the sphere is:

$$x^2 + y^2 + z^2 = r^2 \quad (3.3)$$

Moreover, it is known, from the spherical lens optics, that

$$\frac{1}{p} + \frac{1}{q} = \frac{2}{r_t \sin \vartheta_g} \quad (3.4)$$

and

$$\frac{1}{p} + \frac{1}{q} = \frac{2 \sin \vartheta_g}{r_s} \quad (3.5)$$

where r_t , is the tangential radius, and r_s is the saggital radius. The sphere case have $r_t = r_s$, this mean that, apart from the normal incidence case, the sphere cannot perfectly focalize/collimate a beam. The radius choosen in Surface_conic object is that corresponding to the equation 3.4:

$$r = \frac{2}{\cos \vartheta} \frac{pq}{p+q} \quad (3.6)$$

where p correspond to the object focus length, q to the image lengths, ϑ_g to the incidence angle and $\vartheta = \frac{\pi}{2} - \vartheta_g$.

For the paraboloid shape, to find the correct coefficients that define the right surface, it is needed the incidence angle, one focal distance and another parameter that distinguish between the two behaviour of the mirror that are showed in Figure 3.6a and, Figure 3.6b. This two system correspond mirrors that, physically, have different behaviour, the first one Figure 3.6a, focalize a Beam, the second one, Figure 3.6b, collimate a Beam.

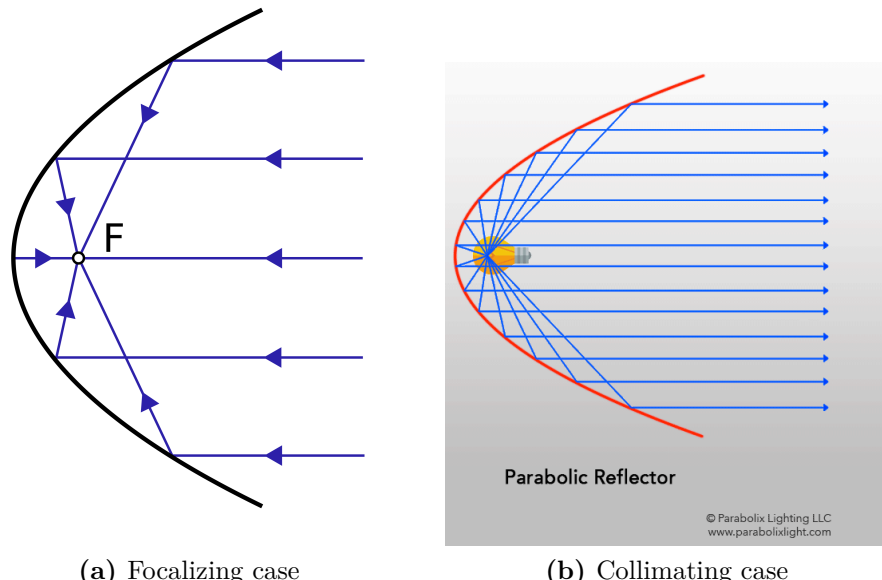


Figura 3.6: Parabola

The general equation of a parabola, such that in Figure 3.7 is

$$y = \frac{1}{4f} x^2 \quad (3.7)$$

where f is the focal distance of the parabola. After a few calculation, see Appendix B, it is possible to correlate f with the input parameter in this sense

$$f = d \sin^2 \vartheta \quad (3.8)$$

where d is the object focal distance, in the case depicted in Figure 3.6a, otherwise, in the case depicted in Figure 3.6b, d is the image focal distance.

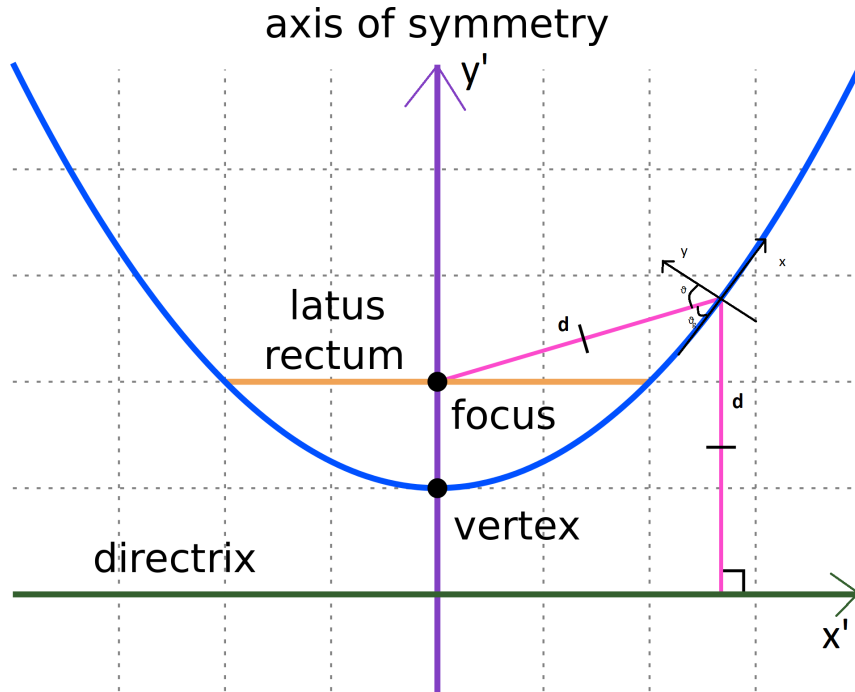


Figura 3.7: System

For the elliptical case the situation is rappresented in Figure 3.8. Equation 3.9 describe the general equation of an ellipse where appear two unknown a and b .

$$\frac{x^2}{a^2} + \frac{y^2}{b^2} = 1 \quad (3.9)$$

It is possible to correlate (Appendix B), the focal distances plus the incidence angle with the two parameters a and b with the following two equations:

$$p = \frac{a + b}{2} \quad (3.10)$$

$$q = \sqrt{ab} \cos \vartheta \quad (3.11)$$

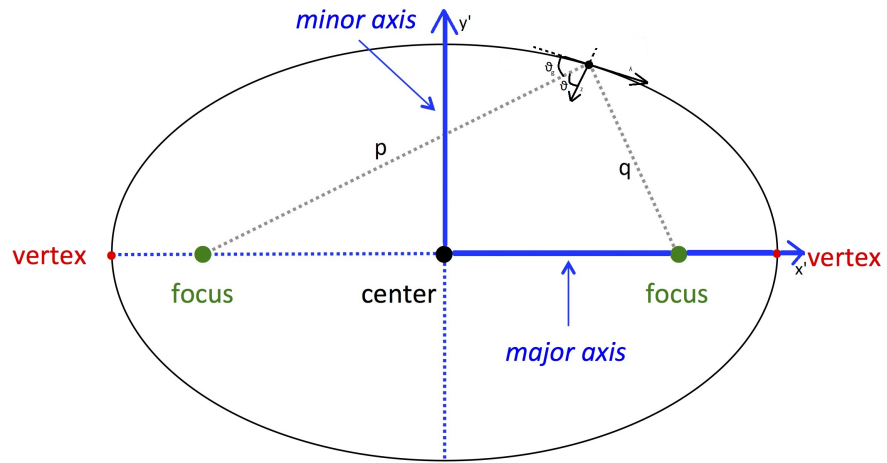


Figura 3.8: Ellipse System

Defined the surface in the $x'y'$, it is done a rotation and a translation in order to center the new xy system on the point P with the normal at that point equal to the z-axis.

For the hyperboloidal mirror the situation is similar to that of the ellipsoidal case, in fact, the general equation of the an hyperbola such the one in Figure is

$$\frac{x^2}{a^2} - \frac{y^2}{b^2} = 1 \quad (3.12)$$

and the equations that correlate the focal distances and the incidence angle with the parameter a and b are

$$p = \frac{a - b}{2} \quad (3.13)$$

$$q = \sqrt{ab} \sin \theta \quad (3.14)$$

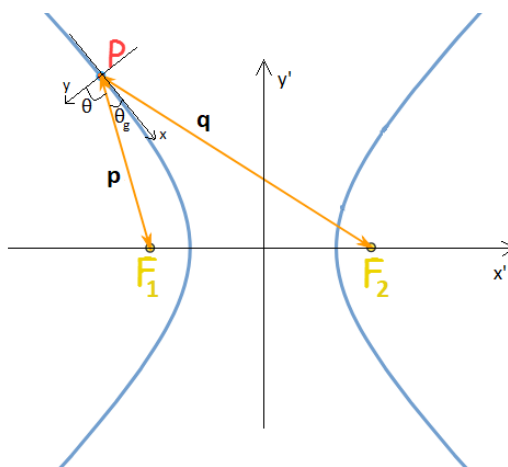


Figura 3.9: Hyperbola System

After that it, as in the case of the ellipsoidal mirror, it need a rotation and a translation to complete the work. For the mirrors, in the program, there is a further

option that make the mirror cylindrical in one dimension maintain its surface conic in the other, to do this, in Surface_conic object, it is defined a function set_cylindrical, that change the shape of the surface, from a complete surface conic, to a surface conic in one dimension and cylindrical in the other.

Apart of the mirrors elements is implement also an ideal lens element that follow the typical lens equation:

$$\frac{1}{f_x} = \frac{1}{p} + \frac{1}{q} \quad (3.15)$$

$$\frac{1}{f_z} = \frac{1}{p} + \frac{1}{q} \quad (3.16)$$

where f_x is the x focal length and f_z is the z focal length. For this optical element the input parameters are the object focal distance, image object distance and the two focal distances (f_x, f_z) that, in the default mode, are setted equal with a value equal to $f_x = f_z = \frac{pq}{p+q}$.

3.2.2 Compound Optical Element (KB and Montel system)

This program include also two different system composed by more mirrors. Starting from conical mirrors, combining them, is possible to have a compound optical elements that can simulate the behaviour of some typical instrumentation that characterize the facilities, in particular in the synchrotron world. The compound optical system implemented are two of those mentioned in Chapter 2:

- KirkPatrickBaez system (KB system)
- Montel

KirkPatrickBaez or, more simply, KB system are shown in Figure 3.10 is composed by two cylindrical surfacing conic mirror placed one after the other with the two focal lens that converge in the same point. There are implemented two different kind of KB system, a first one composed by two elliptical mirrors and a second one composed by parabolic mirrors. The input parameter that the program need are the two incidence angle and the two focal, with respect to the center of the KB system, represented in Figure 3.11 and the separation of the two mirror, from center to center.

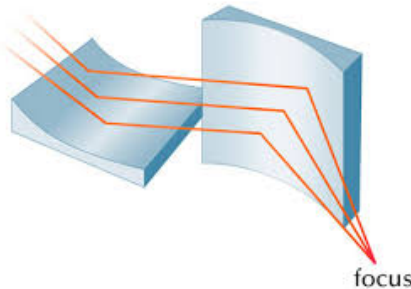


Figura 3.10: System

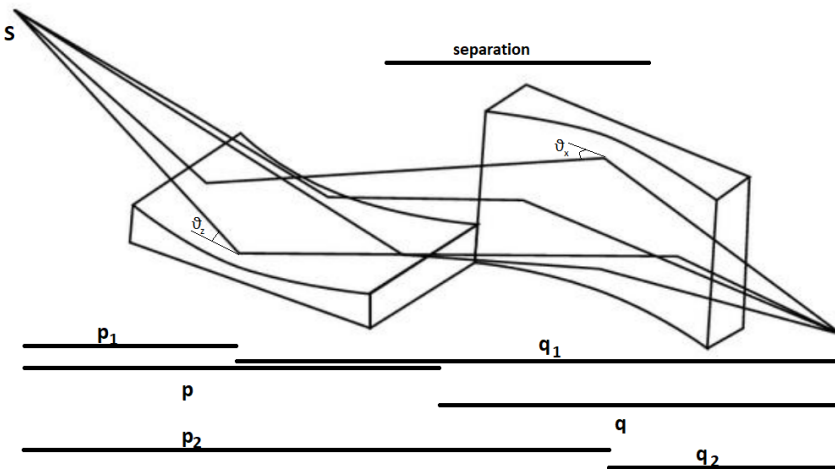


Figura 3.11: System

Because this system is simply a system composed by two surface conical mirror in series the parameter that the system need to define the mirror are not the ones defined by the user but are the focal distance of the two mirrors that are, as shown in Figure, p_1 , q_1 , p_2 , q_2 , These parameter represent the object focal distance (p_1 , p_2) and the image focal distances (q_1 , q_2) of the two mirror, as represented in Figure 3.11. Figure 3.12, show an example of the definition for a KB system that have an object focal length of 2m, an image focal distance of 5m, a separation between the two center of the mirrors of 1m, and the two angle of incidence equal each other to 2° .

```

1  from monwes.CompoundOpticalElement import CompoundOpticalElement
2  import numpy as np
3
4  theta = 88. * np.pi / 180
5  KB = CompoundOpticalElement.initialize_as_kirkpatrick_baez(p=2., q=5., separation=1., theta_z=theta)

```

Figura 3.12: Example 5

The Montel system, depicted in Figure 3.13, is composed, as for the KB, by two surface conical mirror cylindrical in one direction, but, because the two mirror are not in series, as for the case of the KB, the situation is a bit complicate. Starting from definition of the two mirrors one is rotated of 90° , in order to have a mirror in the xy plane, and another one in the zy plane. As shown in Figure 3.13 the center of the Cartesian system is setted in the point where the optical axis of the system hit the compound system having the normal of the first normal equal to the z -axis, and the second normal equal to the $-x$ -axis. The system is defined by the following parameter p , q , ϑ_z , ϑ_x , where p and q are the focal distance of the two mirrors and ϑ_z and ϑ_x are the angle of incidence to define the correct mirrors (by default $\vartheta_z = \vartheta_x$).

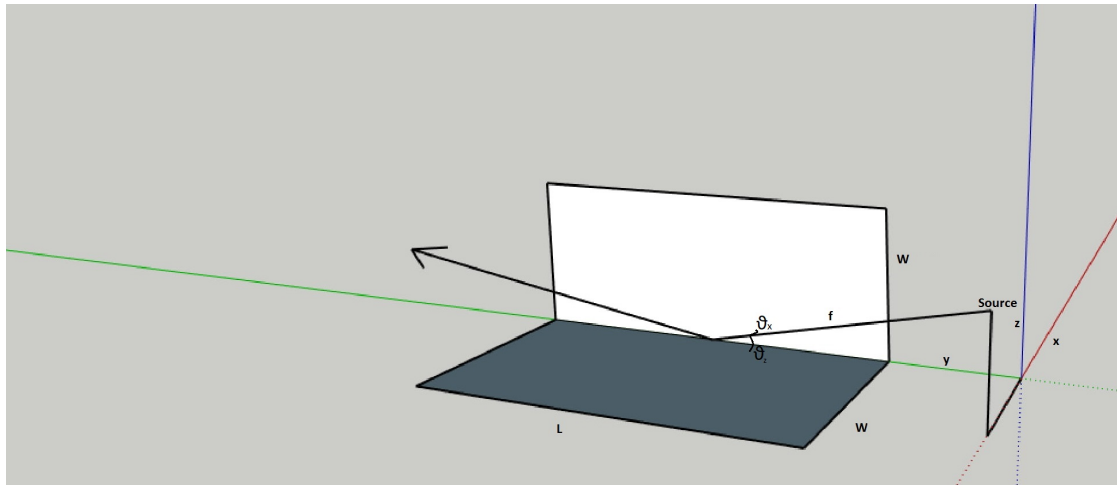


Figura 3.13: System

The following Figure 3.14 show an example code for a parabolic Montel system having an object focal length of 5m, image focal length of 2m and the two incidence angle of 1.5° , that focalize a Beam. As for the KB system also in this case there are implemented two possibilities, an ellipsoidal system (having the two mirror as ellipsoid), and parabolic system (having the two mirror as ellipsoid).

```

1  from monwes.CompoundOpticalElement import CompoundOpticalElement
2  import numpy as np
3
4  theta = 88.5 * np.pi / 180
5  montel = CompoundOpticalElement.initialize_as_montel_parabolic(p=5., q=2., theta_z=theta, infinity_location='p')

```

Figura 3.14: Example 6

3.3 Tracing System

Defined the Beam and the different optical element, to complete a simulation, is needed a tool that put everything together and modify the property of the beam after the interaction with the optical elements.

For example, if it want to simulate the system depicted in Figure 3.15, it have to define a Beam source, the optical element and, at the end, somewhere, the distances between the optical elements. The tracing part of the program, for the non-compound optical element, is written in such a way that the trace work in series, one optical element after the other. This, in series methods, work with the definition of two distances, object/image distance from the center of the optical element, the incidence angle of the Beam, that can be different from the designing one, and a second angle that define the mirror with respect to the Beam. (normally and also for the default case the incidence angle i equal to the designed one, and the second angle is fixed to 0°). One possibilities, to define the systam in Figure 3.15 is to set the object distances of the mirrors equal to distance d_0 and d_1 , and the image distances equal to 0, for the lens lets set the object distance equal to d_3 and the image distance equal to d_4 as it is reported in Figure 3.16.

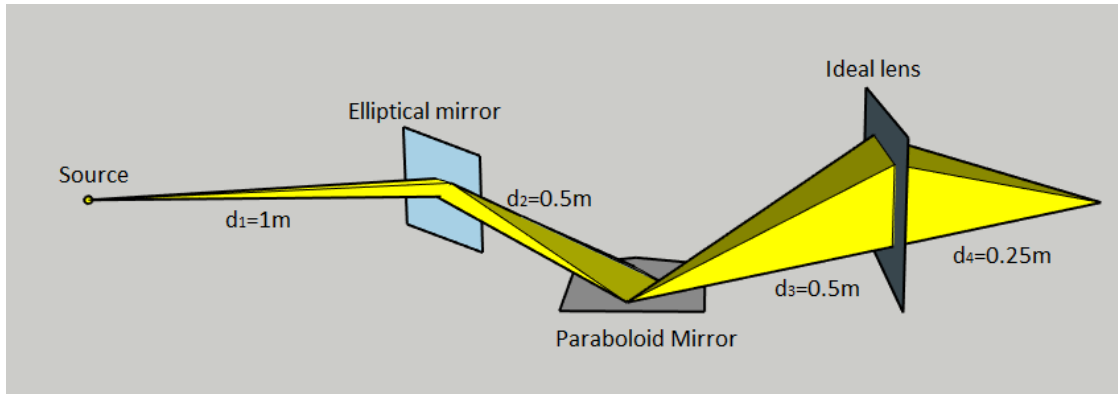


Figura 3.15: System

```

1 import ...
5
6
7 theta_e = 88.5 * np.pi / 180
8 theta_p = 88. * np.pi / 180
9 beam = Beam()
10 beam.set_gaussian_divergence(1e-3, 1e-4)
11
12 ell = Optical_element.initialize_as_surface_conic_ellipsoid_from_focal_distances(p=1., q=2., theta=theta_e)
13 par = Optical_element.initialize_as_surface_conic_paraboloid_from_focal_distances(p=0.5, q=2., theta=theta_p, infinity_location='p')
14 lens = Optical_element.initialize_as_ideal_lens(p=1., q=2.)
15
16 beam = ell.trace_optical_element(beam, p=1., q=0)
17 beam = par.trace_optical_element(beam, p=0.5, q=0., alpha=np.pi/180)
18 beam = lens.trace_optical_element(beam, p=0.5, q=0.25)

```

Figura 3.16: Example 7

3.3.1 Tracing for simple Optical element

Going deeper in the code, the algorithm that trace a single element is divided in 5 step

1. change the reference system with that soldal with the optical element after two rotation, one along x-axis, and second along y-axis, and a translation equal to the object distance of the optical element
2. free propagation up to the optical element
3. effect of the optical element
4. free propagation to the image plane
5. changing the Cartesian system in that one that have the optical axis equal to the y-axis

The first three point are condensed in the method `effect_of_the_optical_element`, that is showed in Figure 3.17a, and the last two point are condensed in the method `effect_of_the_screen` that is showed in Figure 3.17b.

```

227     def effect_of_optical_element(self,beam):
228         self.rotation_to_the_optical_element(beam)
229         self.translation_to_the_optical_element(beam)
230         [beam, t]=self.intersection_with_optical_element(beam)
231         self.output_direction_from_optical_element(beam)
232
235     def effect_of_the_screen(self,beam):
236         self.rotation_to_the_screen(beam)
237         self.translation_to_the_screen(beam)
238         if np.abs(self.q) > 1e-13:
239             self.intersection_with_the_screen(beam)
240

```

(a) Example code for a Gaussian spot

(b) Plot of Figure 3.2a

Figura 3.17: Example 1

Because of the different definition, the tracing method of the rays' beam, need a different interpreter that can link the beam with the different optical elements that meet on his way. Because of the different nature, there are implemented two kind of tracing, a first one that trace the KB system, that is composed by a series of optical elements and so can be used for all the compound optical elements that are in series. And a second one that is specific for the Montel system, because it is not composed by mirrors in series rather than mirrors in parallel, having the two elements in a very small region of the space that have in which order the rays of the beam hit the different mirrors.

3.3.2 Tracing for KB

For KB system the situation is more or less the same as for a simple optical mirrors, with the only difference that there are more than one mirror. So the algorithm to simulate the tracing system is nothing else than a for loop, that use the tracing system of the simple optical element. In this the object and the image distance from the center of the system are the default ones, such as for the incidence angles. Figure 3.18, show the trace code for the compound elements that are in series.

```

372     def trace_compound(self,beam1):
373
374         beam=beam1.duplicate()
375
376         self.system_initialization(beam)
377
378         for i in range_(self.oe_number()):
379
380             if self.oe[i] is not None:
381
382                 self.oe[i].effect_of_optical_element(beam)
383                 self.compound_specification_after_oe(i=i)
384                 self.oe[i].effect_of_the_screen(beam)
385                 self.compound_specification_after_screen(beam = beam, i=i)
386
387         return beam

```

Figura 3.18: Example 8

3.3.3 Tracing for Montel

Montel system is completely different from the KB system and all the series optical system, so it need a new trace system. This new trace system is divided as

follow

1. Changing the reference frame in one having the center on the center of the mirrors, with a z-axis corresponding to the normal of one mirror and -x-axis equal to the normal of the second mirror. This transformation is done in a similar way of the normal tracing, two rotation of the beam, and one translation, differently from the normal tracing, the tw rotation are done such that the beam hit the mirrors with an incidence angle set by the user
2. Focus the attention on the travel time of each ray in order to know which is the nearest optical element of each ray
3. free propagation of each ray up to the nearest optical element
4. effect of the system for each ray
5. repeat the 2nd, 3rd and 4th passage two times, in order to consider the two reflection
6. Change the reference system solidale with the beam that is subject to two reflection, doing two rotation and one translation

What is reported above is the default tracing system that, because of its centrality on my thesis' work have many option. What is setted by the user is

1. focal distances and incidence angles, that define the two rotation and the translation of the tracing system
2. name of the File in which is saved the data of the simulation, by default no data is saved
3. there is the possibility to choose a different point, from the origin, in which the the optical axis hit the system
4. there is also the possibility to have a final output frame that is not solidal by the two-reflected beam, but with the non reflected beam or with the other two beam that are reflected only one time
5. It is also the possibility to figure out the footprint of the two reflected beam on the system. For clarity the beam that hit the first mirror and after the second is labelled with red point, the beam that hit the second and after first mirror is labelled by blue color

These options are added in order to study better the behaviour of a beam with a Montel system. The possibilities to change the angle of incidence and to hit different part from the origin can be used to study what happen to a beam when is not aligned, or not perfectly aligned, and use these result to align the system in the laboratories. The possibilities to save a File is useful in particular in those case where there is a huge computational effort that need a lot of time, in these cases is possible to work with the result of a big simulation without reappointing it, and so

save time. Figure 3.19 show the code that trace a Montel elements, containing also the special option that were defined above.

```
681
682
683
684     def trace_montel(self, beam, name_file=None, mode=0, p=None, q=None, theta_z=None, theta_x=None, hitting_point=Vector(0., 0., 0.),
685             output_frame=0, print_footprint=1):
686
687         self.oe[0].set_parameters(p=p, q=q, theta=theta_z)
688         self.oe[1].set_parameters(p=p, q=q, theta=theta_x)
689
690         v_in = self.get_optical_axis_in(mode)
691
692         self.input_frame(beam, v_in, mode, hitting_point)
693
694         beam1, beam2, beam3 = self.apply_specular_reflections(beam, name_file, print_footprint)
695
696         if output_frame == 0:
697             v_out = self.get_optical_axis_out(mode)
698         elif output_frame == 1:
699             v_out = v_in
700
701         self.output_frame(beam3[0], v_out, mode)
702         self.output_frame(beam3[1], v_out, mode)
703         self.output_frame(beam3[2], v_out, mode)
704
705
706
707
708
709
710
711
712
713
714
715
716
717
718
719
720
721
722
723
724
725
726
727
728
729
730
731
732
733
734
735
736
737
738
739
740
741
742
743
744
745
746
747
748
749
750
751
752
753
754
755
756
757
758
759
760
761
762
763
764
765
766
767
768
769
770
771
772
773
774
775
776
777
778
779
780
781
782
783
784
785
786
787
788
789
790
791
792
793
794
795
796
797
798
799
800
801
802
803
804
805
```

Figura 3.19: Example 8

Capitolo 4

Results

“Terence: Ma scusa di che ti preoccupi, i piedipiatti hanno altro a cui pensare, in questo momento stanno cercando due cadaveri scomparsi

Bud: Se non spegni quella sirena uno di quei due cadaveri scomparsi lo trovano di sicuro!”

Nati con la camicia

4.1 Testing

To demonstrate the correct behaviour of the program there are done a comparison with respect to the OASYS software for ray tracing simulation, developed by Manuel Sanchez Del Rio, and with respect to the paper [RKM15]. The comparison with OASYS check the correct working of all the component apart from Montel system (mirrors, lens, KB ...), on the contrary, the paper is dedicate for the Montel simulation, because this particular kind of optical system, is not implemented on OASYS.

4.1.1 Testing with OASYS

OASYS (OrAnge SYnchrotron Suite) is a graphical environment for optic simulation used in synchrotron facilities based on orange 3, developped by Manuel Sanchez Del Rio (ESRF) and Luca Rebuffi (ELETTRA). The comparison between the program and the OASYS software is done with the system in Figure 4.1, where the 1st optical system collimate the source, the 2nd optical system focalize the mean at the image plane, the system beewtween the source and the 1st optical system correspond to the focal distance of the system $d_1 = f = 0.4m$, between the 12st and the 2nd optical system thre is a distance $d_2 = 0.6m$ and the distance beetween the 2nd the 2nd and the image plane correspond to the focal length of the 2nd optical system that is $d_3 = f = 0.4$. A system that have parameters defined as before, make a copy of the source image at the image plane. The source parameter used are showed in Figure 4.2, and correspond to a square source spot of $1\mu m^2$, and a initial Gaussian divergence with a FWHM of $1mrad$. The tests are done using different optical system, with the same focal length and, for the mirror it is

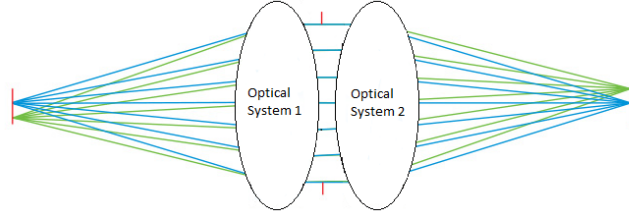


Figura 4.1: Optical system

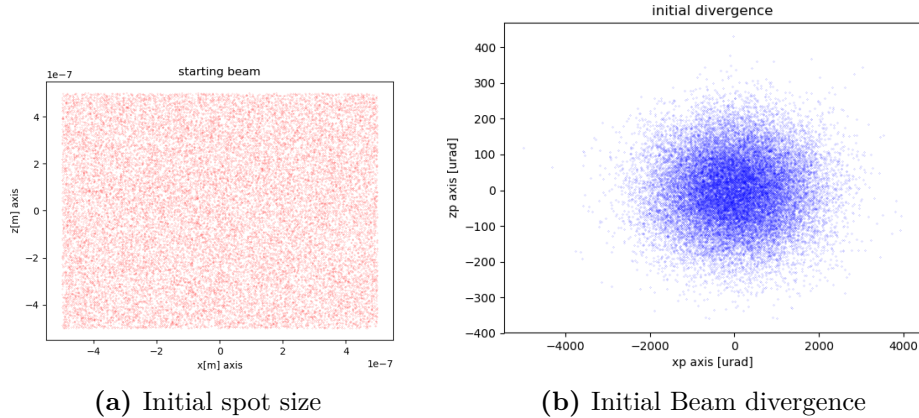


Figura 4.2: Parameter of the source used for the comparison with OASYS

used a grazing incidence angle of $\vartheta = 1.719^\circ$. Below are plotted the image of the Beam at the image plane, putting the OASYS' results on the right, and my results on the left. The system simulated are done with:

1. ideal lenses Figure 4.3
2. parabolic mirror Figure 4.4
3. KB system Figure 4.5

As it is showed in the figures, the result are pretty similar, with an image that depend on the kind of the system, with the ideal lenses the image is perfect, with KB and paraboloid, the image is similar to the original but degrades with the propagation.

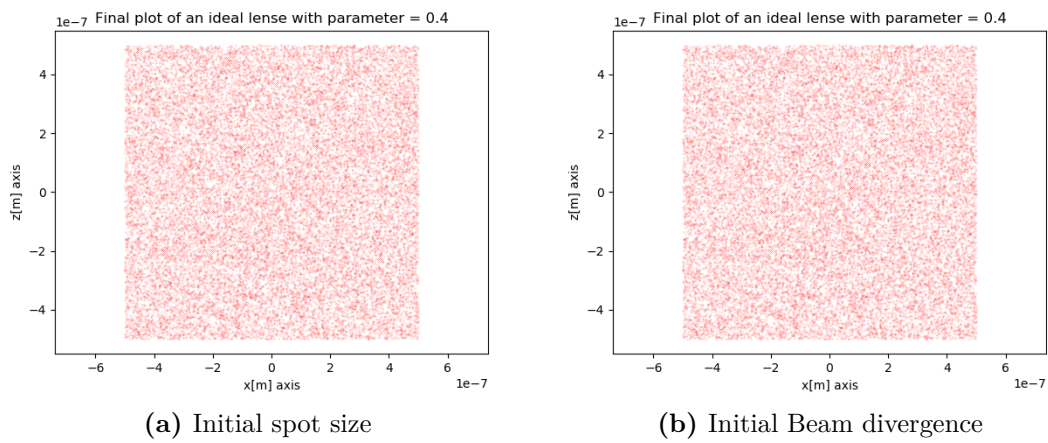


Figura 4.3: Parameter of the source used for the comparison with OASYS

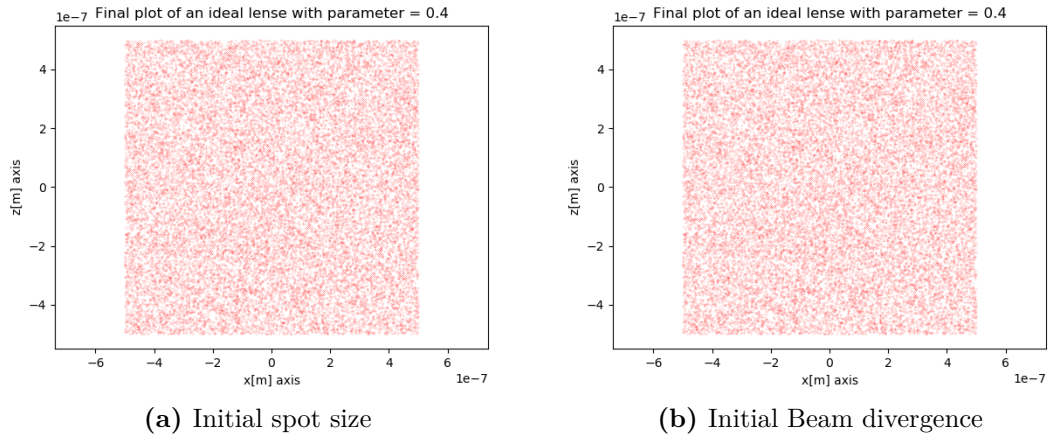


Figura 4.4: Parameter of the source used for the comparison with OASYS

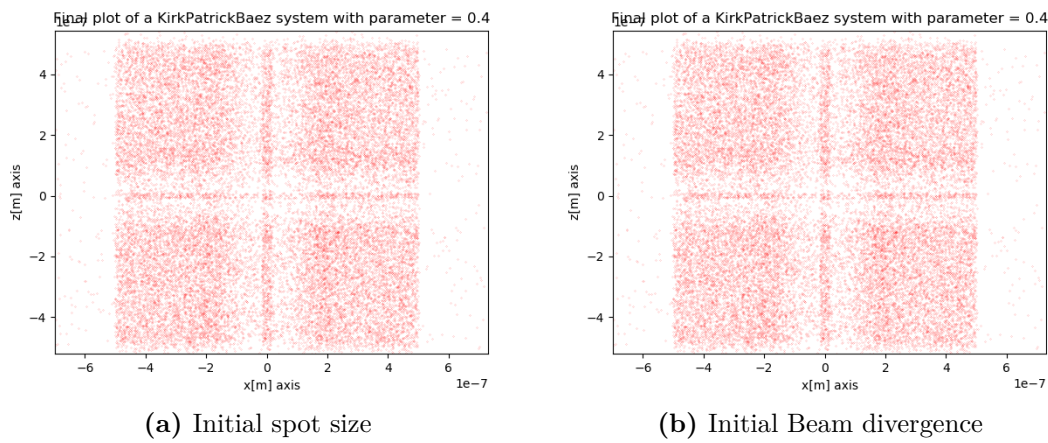


Figura 4.5: Parameter of the source used for the comparison with OASYS

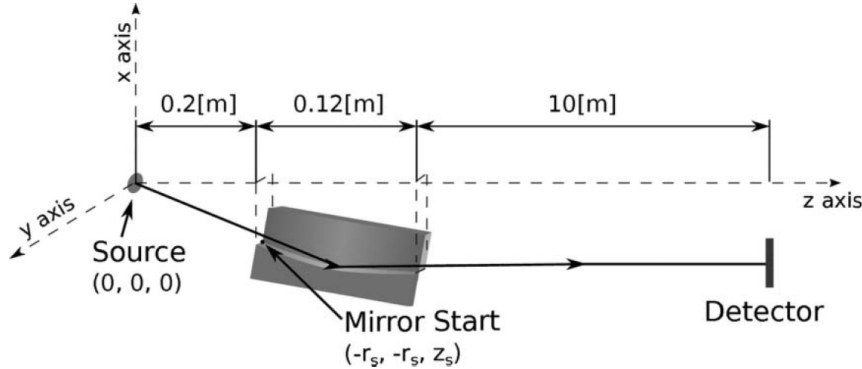


Figura 4.6: Illustration of the Montel system used as a collimator in the paper [RKM15]

4.1.2 Testing with the paper

In Figure 4.6 is depicted the Montel system used in the simulation done by the paper in its system of reference. The aim of this system is to collimate a Beam using a Montel with two parabolic mirrors. The source used have a Gaussian dimension with a FWHM of $2.5\mu\text{m}$ and a Gaussian divergence of 5mrad . The distances, between the source/image plane and the center of the Montel are, respectively, $\simeq 0.26\text{m}$ and 10.06m , moreover, the incidence angle of the Beam is $\vartheta_g \simeq 2.86^\circ$. The result, at the image plane, of the beam size and beam divergence, after the double-reflection of the Montel system, is showed in Figure 4.7. Where, in Figure 4.7a, is showed the figure of the beam at the image plane, and, in Figure 4.7c, is showed the divergence. The quantitative values reported on the paper correspond to a Gaussian-like distribution with a spacial FWHM of $\sim 0.7\text{mm}$, for the spot size, and a FWHM of the Gaussian divergence $\sim 0.01\text{ mrad}$.

Repeating the simulation with my program using the parameter defined in in the paper [RKM15], are figured out in Figure 4.7. As it is showed in the Figure 4.7 there are a qualitative good agreement with the two simulation .Also, under a quantitative point of view, there is a good agreement in fact, in my simulation are obtained a value of $\sim 1\text{mm}$ of FWHM of image size, pretty similar to the one of the other simulation, and $\sim 0.01\text{ mrad}$ FWHM of divergence that is equal to the one obtained with the other simulation.

4.2 Analysis of Montel system

In this section it is done, using the Montel tools devolopped, a study of the Montel effect with respect to a Beam, simulating different situation. The first point, to understand that Montel work well, it is simulated the behaviour of a pointwise source with a certain divergence, using a collimating system, and watching what happen to the beam. The second step is to simulate a collimating beam with a certain source shape geometry and figure out the image plot obtained by a focalizing system in its image plane. What is expected is a point, in the velocity space for the first situation and in the real space for the second simulation, because this is the behaviour of an ideal collimating/focalizing system. For the simulation are

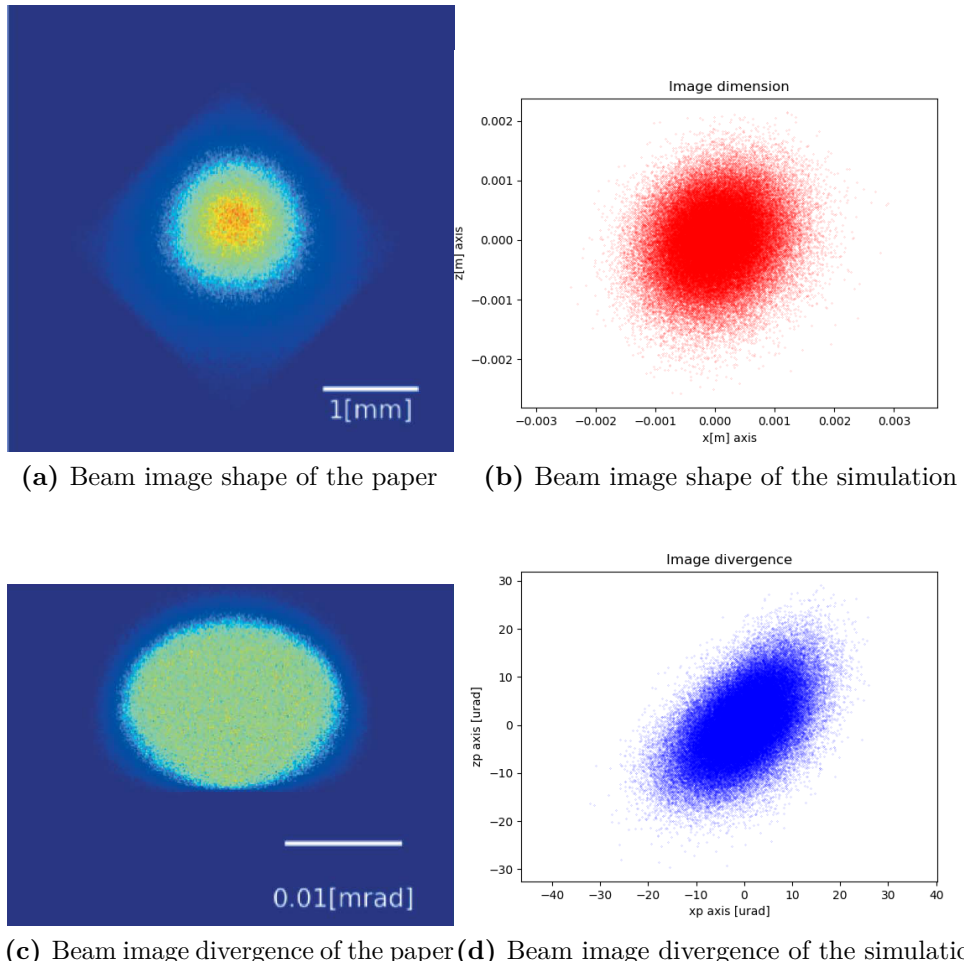


Figura 4.7: Results of the Montel simulations with a source beam with a FWHM spot of $2.5\mu\text{m}$ and a Gaussian divergence of 5mrad

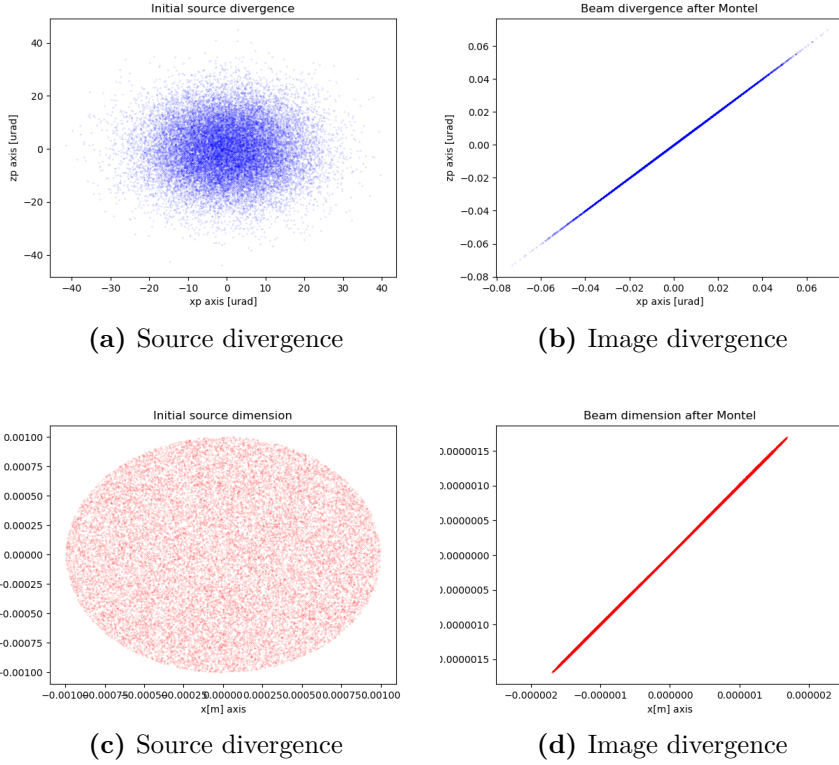


Figura 4.8: Ideal system

used parabolical Montel and an incidence angle of 2° (the choice of the angle is arbitrary, that of the parabolic system is because it is needed to collimate a beam, also for elliptical system is possible to focalize a beam using one focal distance very big).

In Figure 4.8 are reported the results for the ideal collimating/focalizing cases. For the collimating system is used a point wise source with a Gaussian divergence of FWHM of $25\mu\text{m}$, 4.8a, to the image plane. As it is shown there is a collimation, but not perfect, this effect is one limit of the Montel because the perpendicular geometry is not the ideal one. Moreover, for the focalizing system, it is used a circular source spot having a radius of 1mm, 4.8c, with a collimated beam, that shows, at the image plane 4.8d, a similar behaviour as for the collimation case, for the same reason. Another interesting point to show is the footprint on the two mirrors that are represented in Figure 4.9. It is possible to note that the area hit by the beam has a greater component on the y direction (due to the grazing incidence), than in the other direction. In this particular case the x-length of the xy-mirror, and the z-length of the zy-mirror, is very small (at the order of $20\mu\text{m}$) with respect to the y-length that is $\sim 20\text{mm}$. These calculations are done for a very small Gaussian spot with a FWHM of $1\mu\text{m}$ and a narrow divergence of FWHM equal to $25\mu\text{rad}$. Up to know the dimensions of the Montel were not considered, the Montel is set to have infinite dimensions in all the directions. This approach holds in the case of a small source and a narrow profile divergence, otherwise, for example of an isotropic source that can be modelled with a very big divergence the

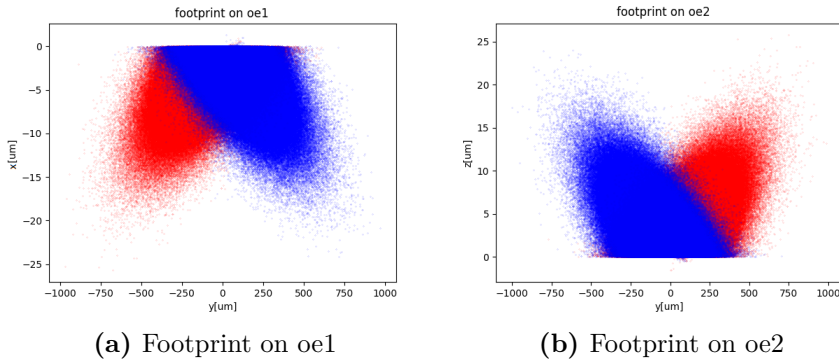


Figura 4.9: Footprint, on the xy-mirror (4.13a) and on zy-mirror (4.13b). The red dots are those rays that hit before xy-mirror and after zy-mirror, the blue ones hit first xy-mirror and after zy-mirror.

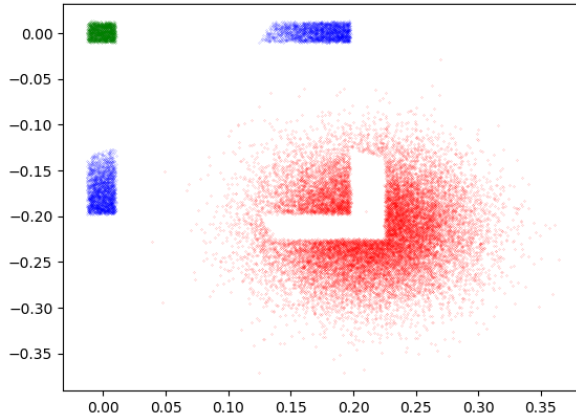


Figura 4.10: Illumination at the image plane of the different Beam (red dots correspond to np-reflected rays, blue dot to one-reflected rays, green dots to two-reflected rays).

situation change. In this section, it is used a Beam source with a square shape with a side of 1mm, with a Gaussian profile divergence of FWHM=1mrad in order to show what happen to the Montel where it is covered over all its surface. The focalizing parabolic Montel parameter are:

- object distance: 1m
- image distance: 3m
- incidence angle: 2°
- length of the Montel: 0.1m
- width of the Montel: 20cm

Figure 4.10, show thee image plane of the Montel defined above. This plot show 4 figure, the biggest one, reppresented by the red dots, correspond to the rays

that reach the image plane without touch the Montel, the rays coloured in blue, are those which are subject to only one reflection that are positioned in different part of the image plane depending which mirror meet, those that hit the xy-mirror correspond to the beam elongated along z, the zy-mirror correspond to the beam elongate along x. At the end, the green dots, are the rays that do both reflection and are centred to the center of the image plane by definition of it.

4.2.1 Alignment

Alignment of a beam is important for experimental use so, this section studies the behaviour of a beam when the beam is not perfectly align, in order to understand the behaviour of the beam in the different cases and act consequently.

The parameter that are changed are :

1. orthogonality
2. incidence angle
3. point of incidence

Using a focusing parabolic Montel system with a source of square shape having a side of $1\mu\text{m}$, and a Gaussian divergence with FWHM of $25\mu\text{m}$

4.2.2 Alignment: Orthogonality

In this section is it done an orthogonality studies of the Montel system, it is studied the behaviour of a beam, using a source parameter defined before. Figure 4.11b presents the interesting histogram versus the horizontal angle x' when the angle between the mirrors change ($\alpha = 90^\circ + \Delta$). It can be noted a improvement of the collimation of the beam changing the angle in the case of closer mirrors ($\Delta = -0.004^\circ$).

Figure show the trend of the FWHM of the x' changing the angle Δ , it is possible to note a minimum for negative angle (this situation correspond to the indigo line) after that the situation become worse. Moreover, the behaviour of the FWHM is not symmetric with respect to 0° , in case of negative angle deviation the situation improve for small range of deviation angle, after that, the trend get worse, on the opposite way, the situation get worse increasing the positive deviation angle.

4.2.3 Alignment: Incidence angle

To understand the behaviour of a non aligned beam it is simulated the situation of a beam that arrive at the Montel system with the wrong angle. In this particular case the system is defined as follow: incidence angle of 3° , square spot of $100\mu\text{ m}^2$, Gaussian divergence with FWHM of $25\mu\text{rad}$. Figure

4.2.4 Alignment: point of incidence

Another way that can be studied to align correctly a beam, is to study the behaviour of a non centred beam with respect to the center of the Montel system.

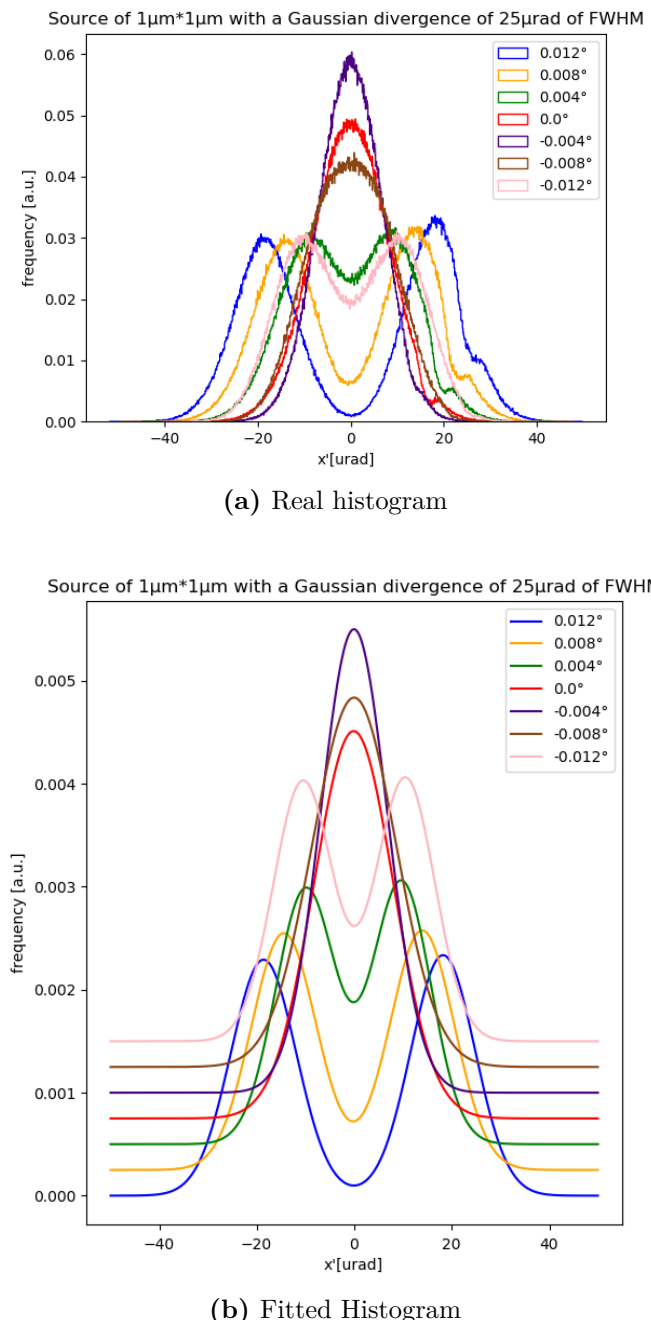


Figura 4.11: Histogram of x' after Montel

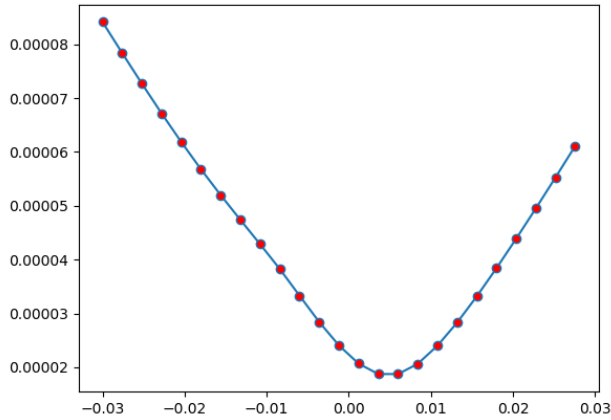


Figura 4.12: FWHM of x' after the Montel changing the orthogonality

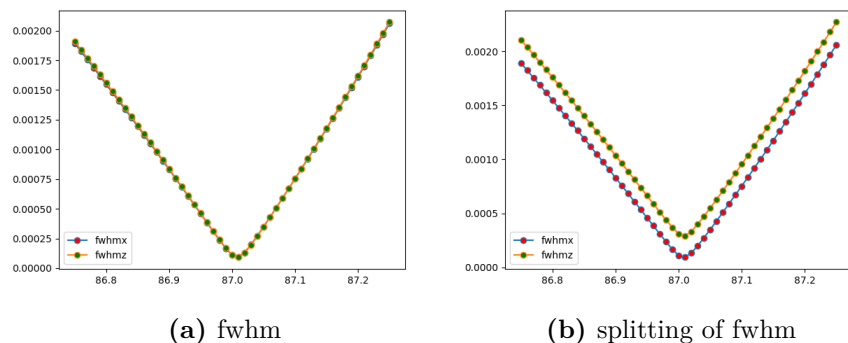


Figura 4.13: Incidence angle

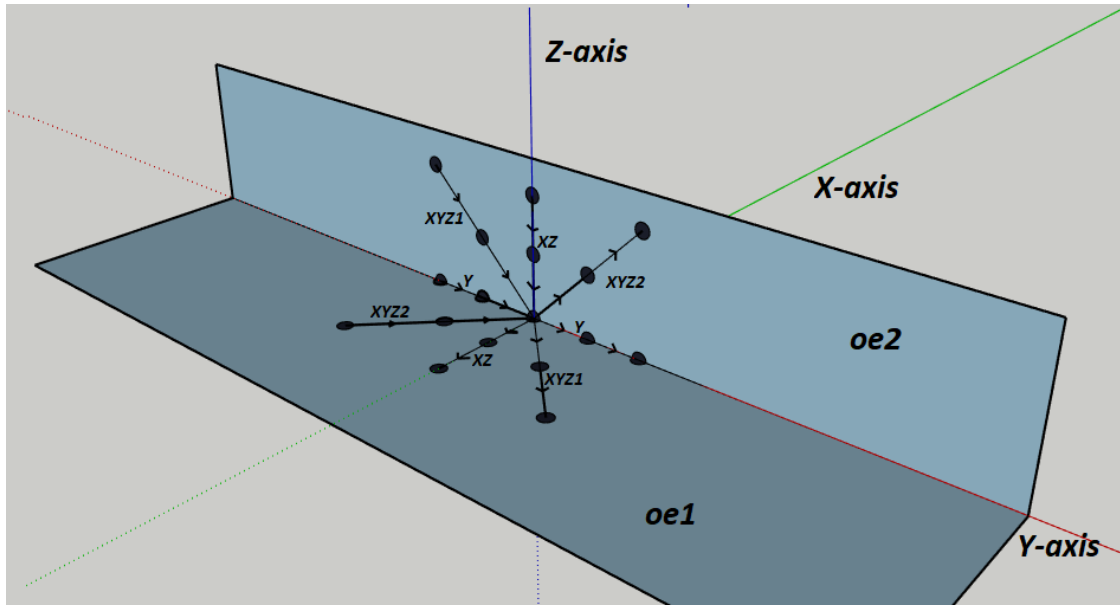


Figura 4.14: Different path for simulate the non-centred beam

In this section is reported the behaviour about the change of FWHM of both x' and z' following different path. Figure 4.14 show the different path followed to simulate the non-centred beam that are named:

1. Y
2. XZ
3. XYZ1
4. XZY2

Figure 4.15 show the behaviour of the two FWHM of the beam changing the incidence point of the beam moving the different paths. This point is defined with respect to the center of the Montel system that correspond to the origin (0, 0, 0). In Figure 4.16a, the incidence point move along y-axis, start from the point (0, 1.5mm, 0) and arriving to the point (0, -1.5mm, 0), and show, more or less, a flat behaviour of the FWHM. Figure 4.16b start from the point (0, 0, 0.15mm) and arrive to (-0.15mm, 0, 0) and have specular behaviour for the two FWHM, there is a minimum of the two FWHM near the origin point, moving on the oe1 worse the FWHM of z' and maintain the other constant, on the contrary, moving on the oe2 the situation is reversed, in this case the FWHM of x' get worse, maintaining constant the one of z' . Figure 4.16c start from (0, 1.5mm, 0.15mm) and arrive to (-0.15mm, -1.5mm, 0) and Figure 4.16d start from (-0.15mm, 1.5mm, 0) and arrive to (0., -1.5mm, 0.15mm). The behaviour of this last two path are similar to that of 4.16b, this is reasonable, because the motion along y-axis does not influence the FWHM because of the definition of the cylindrical mirror, that in any point along the y direction have the same geometry. In Figure 4.16 it is show the intensity profile of the two-reflection beam after the Montel, calculated as the number of the rays in the two-reflection beam with respect to the initial number of rays. The

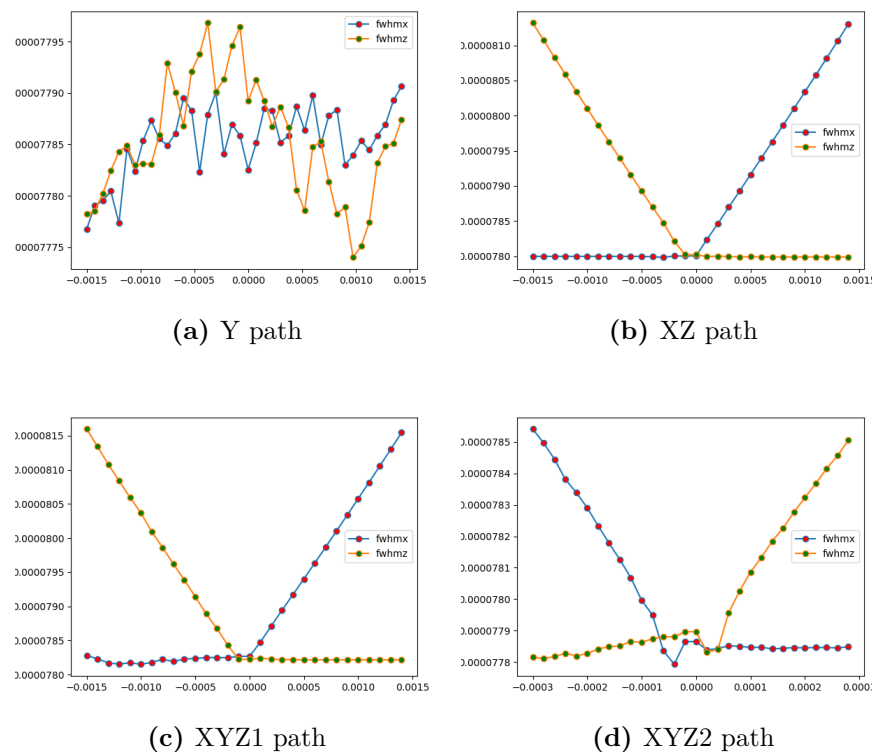


Figura 4.15: Results of the Montel system of a source beam with a FWHM spot of $2.5\mu\text{m}$ and a Gaussian divergence of 5mrad

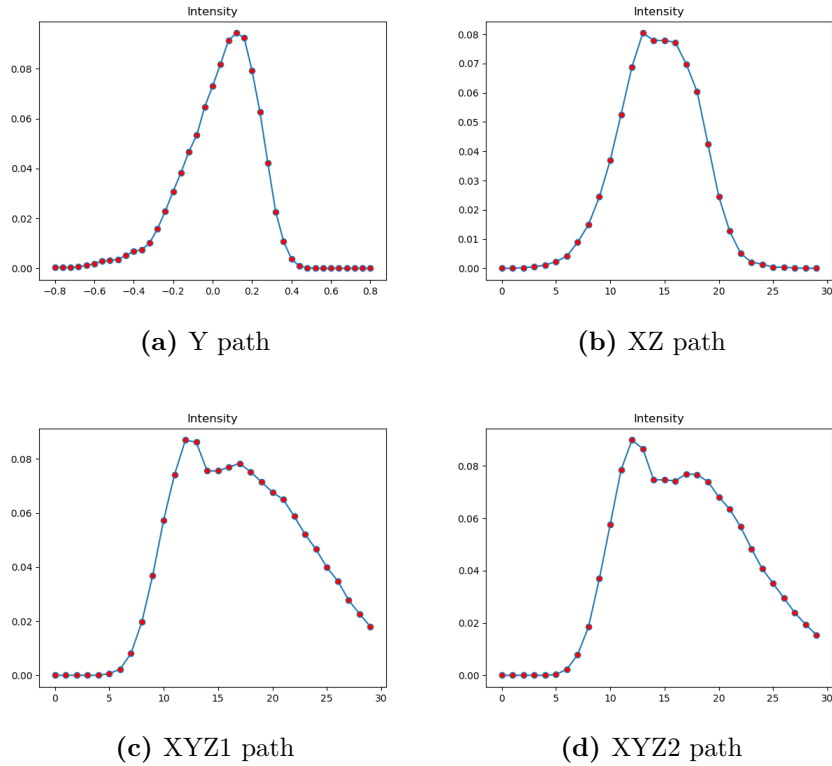


Figura 4.16: Results of the Montel system of a source beam with a FWHM spot of $2.5\mu\text{m}$ and a Gaussian divergence of 5mrad

source used, in this case, correspond to a big spot of a square geometry with an area of 1mm^2 , and a large Gaussian divergence with a FWHM of 10mrad . The Montel used is a parabolic localizing system having an object distance of 1m , an image distance of 3m , an incidence angle of 2° and a finite dimension, with a length of 20cm and a width of 2cm . The different path move along these points; $\text{ymax}=50\text{cm}$, $\text{ymin}=-50\text{cm}$, $\text{xmin}=-2\text{cm}$, $\text{xmax}=0$, $\text{zmax}=2\text{cm}$, $\text{zmin}=0$

The plots in Figure 4.16, are interesting, because represent the intensity of the "green" Beam in Figure 4.10, that can be directly measured and so, it is possible to realted the centring of the Beam calculating the intensity of this Beam.

Appendice A

Table for absorption coefficients

Table A. report the X-Ray Mass Attenuation Coefficients. Material constants assumed in the present evaluations for elemental media. Values are given for the ratio of atomic number-to-mass Z/A , the mean excitation energy I , and the density ρ . Some density values are only nominal; those for $Z = 85$ and 87 were arbitrarily set to 10 in order to complete the calculations.

Z	Element		Z/A	I [eV]	Density $\frac{[g]}{[cm^3]}$
1	H	Hydrogen	0.99212	19.2	8.375E-05
2	He	Helium	0.49968	41.8	1.663E-04
3	Li	Lithium	0.43221	40.0	5.340E-01
4	Be	Beryllium	0.44384	63.7	1.848E+00
5	B	Boron	0.46245	76.0	2.370E+00
6	C	Carbon, Graphite	0.49954	78.0	1.700E+00
7	N	Nitrogen	0.49976	82.0	1.165E-03
8	O	Oxygen	0.50002	95.0	1.332E-03
9	F	Fluorine	0.47372	115.0	1.580E-03
10	Ne	Neon	0.49555	137.0	8.385E-04
11	Na	Sodium	0.47847	149.0	9.710E-01
12	Mg	Magnesium	0.49373	156.0	1.740E+00
13	Al	Aluminum	0.48181	166.0	2.699E+00
14	Si	Silicon	0.49848	173.0	2.330E+00
15	P	Phosphorus	0.48428	173.0	2.200E+00
16	S	Sulfur	0.49897	180.0	2.000E+00
17	Cl	Chlorine	0.47951	174.0	2.995E-03
18	Ar	Argon	0.45059	188.0	1.662E-03
19	K	Potassium	0.48595	190.0	8.620E-01
20	Ca	Calcium	0.49903	191.0	1.550E+00
21	Sc	Scandium	0.46712	216.0	2.989E+00
22	Ti	Titanium	0.45948	233.0	4.540E+00
23	V	Vanadium	0.45150	245.0	6.110E+00

Z	Element		Z/A	I [eV]	Density $\frac{[g]}{[cm^3]}$
24	Cr	Chromium	0.46157	257.0	7.180E+00
25	Mn	Manganese	0.45506	272.0	7.440E+00
26	Fe	Iron	0.46556	286.0	7.874E+00
27	Co	Cobalt	0.45815	297.0	8.900E+00
28	Ni	Nickel	0.47708	311.0	8.902E+00
29	Cu	Copper	0.45636	322.0	8.960E+00
30	Zn	Zinc	0.45879	330.0	7.133E+00
31	Ga	Gallium	0.44462	334.0	5.904E+00
32	Ge	Germanium	0.44071	350.0	5.323E+00
33	As	Arsenic	0.44046	347.0	5.730E+00
34	Se	Selenium	0.43060	348.0	4.500E+00
35	Br	Bromine	0.43803	343.0	7.072E-03
36	Kr	Krypton	0.42959	352.0	3.478E-03
37	Rb	Rubidium	0.43291	363.0	1.532E+00
38	Sr	Strontium	0.43369	366.0	2.540E+00
39	Y	Yttrium	0.43867	379.0	4.469E+00
40	Zr	Zirconium	0.43848	393.0	6.506E+00
41	Nb	Niobium	0.44130	417.0	8.570E+00
42	Mo	Molybdenum	0.43777	424.0	1.022E+01
43	Tc	Technetium	0.43919	428.0	1.150E+01
44	Ru	Ruthenium	0.43534	441.0	1.241E+01
45	Rh	Rhodium	0.43729	449.0	1.241E+01
46	Pd	Palladium	0.43225	470.0	1.202E+01
47	Ag	Silver	0.43572	470.0	1.050E+01
48	Cd	Cadmium	0.42700	469.0	8.650E+00
49	In	Indium	0.42676	488.0	7.310E+00
50	Sn	Tin	0.42120	488.0	7.310E+00
51	Sb	Antimony	0.41889	487.0	6.691E+00
52	Te	Tellurium	0.40752	485.0	6.240E+00
53	I	Iodine	0.41764	491.0	4.930E+00
54	Xe	Xenon	0.41130	482.0	5.485E-03
55	Cs	Cesium	0.41383	488.0	1.873E+00
56	Ba	Barium	0.40779	491.0	3.500E+00
57	La	Lanthanum	0.41035	501.0	6.154E+00
58	Ce	Cerium	0.41395	523.0	6.657E+00
59	Pr	Praseodymium	0.41871	535.0	6.710E+00
60	Nd	Neodymium	0.41597	546.0	6.900E+00
61	Pm	Promethium	0.42094	560.0	7.220E+00
62	Sm	Samarium	0.41234	574.0	7.460E+00
63	Eu	Europium	0.41457	580.0	5.243E+00
64	Gd	Gadolinium	0.40699	591.0	7.900E+00
65	Tb	Terbium	0.40900	614.0	8.229E+00
66	Dy	Dysprosium	0.40615	628.0	8.550E+00
67	Ho	Holmium	0.40623	650.0	8.795E+00
68	Er	Erbium	0.40655	658.0	9.066E+00
69	Tm	Thulium	0.40844	674.0	9.321E+00
70	Yb	Ytterbium	0.40453	684.0	6.730E+00
71	Lu	Lutetium	0.40579	694.0	9.840E+00

Z	Element		Z/A	I [eV]	Density $\frac{[g]}{[cm^3]}$
72	Hf	Hafnium	0.40338	705.0	1.331E+01
73	Ta	Tantalum	0.40343	718.0	1.665E+01
74	W	Tungsten	0.40250	727.0	1.930E+01
75	Re	Rhenium	0.40278	736.0	2.102E+01
76	Os	Osmium	0.39958	746.0	2.257E+01
77	Ir	Iridium	0.40058	757.0	2.242E+01
78	Pt	Platinum	0.39984	790.0	2.145E+01
79	Au	Gold	0.40108	790.0	1.932E+01
80	Hg	Mercury	0.39882	800.0	1.355E+01
81	Tl	Thallium	0.39631	810.0	1.172E+01
82	Pb	Lead	0.39575	823.0	1.135E+01
83	Bi	Bismuth	0.39717	823.0	9.747E+00
84	Po	Polonium	0.40195	830.0	9.320E+00
85	At	Astatine	0.40479	825.0	1.000E+01
86	Rn	Radon	0.38736	794.0	9.066E-03
87	Fr	Francium	0.39010	827.0	1.000E+01
88	Ra	Radium	0.38934	826.0	5.000E+00
89	Ac	Actinium	0.39202	841.0	1.007E+01
90	Th	Thorium	0.38787	847.0	1.172E+01
91	Pa	Protactinium	0.39388	878.0	1.537E+01
92	U	Uranium	0.38651	890.0	1.895E+01

Appendice B

How to calculated the ellipse's and hyperbola's coefficients

For the ellipse showed in Figure B.1, the ellipse is defined as:

$$\left(\frac{x'}{a}\right)^2 + \left(\frac{y'}{b}\right)^2 = 1 \quad (\text{B.1})$$

with

$$c^2 = a^2 - b^2 \quad (\text{B.2})$$

Because the ellipse is the curve in a plane surrounding two focal points such that the sum of the distances to the two focal points is constant for every point, so:

$$p + q = (c + a) + (a - c) = 2a \quad (\text{B.3})$$

Thus

$$a = \frac{p + q}{2} \quad (\text{B.4})$$

Now, considering the triangle $AA'P$, using the law of cosines, and substituting with the equations above:

$$4c^2 = p^2 + q^2 - 2pq\cos(2\vartheta) \quad (\text{B.5})$$

$$4(a^2 - b^2) = p^2 + q^2 - 2pq\cos(2\vartheta) \quad (\text{B.6})$$

$$(p + q)^2 - 4b^2 = p^2 + q^2 - 2pq\cos(2\vartheta) \quad (\text{B.7})$$

$$b^2 = \frac{2pq(1 + \cos(2\vartheta))}{4} \quad (\text{B.8})$$

$$b = \sqrt{pq}\cos(\vartheta) \quad (\text{B.9})$$

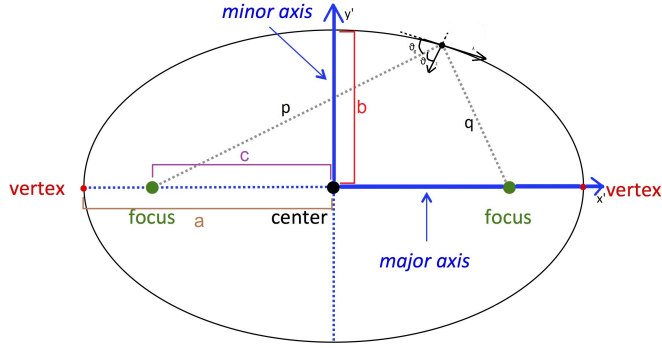


Figura B.1: Hyperbola's system

For the Hyperbola the situation is similar. For the system in Figure B.2, the equation of the parabola is

$$\left(\frac{x'}{a}\right)^2 - \left(\frac{y'}{b}\right)^2 = 1 \quad (\text{B.10})$$

with

$$c^2 = a^2 + b^2 \quad (\text{B.11})$$

In this case the definition of hyperbola is the curve in a plane surrounding two focal points such that the difference of the distances to the two focal points is constant for every point, so:

$$p - q = (c + a) - (c - a) = 2a \quad (\text{B.12})$$

Thus

$$a = \frac{p - q}{2} \quad (\text{B.13})$$

As before, considering the triangle F_1F_2P , using the law of cosines, and substituting with the equations above:

$$4c^2 = p^2 + q^2 - 2pq\cos(2\vartheta_g) \quad (\text{B.14})$$

$$4(a^2 + b^2) = p^2 + q^2 - 2pq\cos(2\vartheta_g) \quad (\text{B.15})$$

$$(p - q)^2 + 4b^2 = p^2 + q^2 - 2pq\cos(2\vartheta_g) \quad (\text{B.16})$$

$$b^2 = \frac{2pq[1 - \cos(2\vartheta_g)]}{4} \quad (\text{B.17})$$

$$b = \sqrt{pq}\sin(\vartheta_g) = \sqrt{pq}\cos(\vartheta_g) \quad (\text{B.18})$$

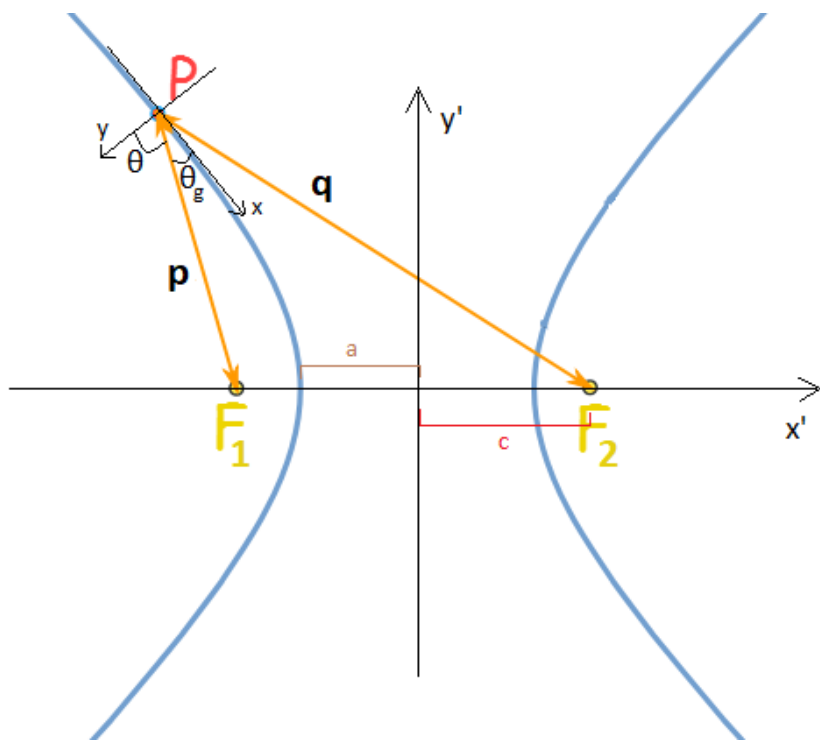


Figura B.2: Hyperbola's system

Bibliografia

- [Dal16] Daniele Dallacasa. Processi di radiazione e mhd, 2016.
- [Fit06] Richard Fitzpatrick. Rayleigh scattering, 2006.
- [Mic86] A.G. Michette. *Optical systems for soft X rays*. Plenum Press, 1986.
- [RKM15] Giacomo Resta, Boris Khaykovich, and David Moncton. Nested kirkpatrick–baez (montel) optics for hard x-rays. *Journal of Applied Crystallography*, 48(2):558–564, 2015.
- [Uni16] Boston University. *Compton Scattering*, 2016.